Annual Review of Biophysics

Simulation of Complex Biomolecular Systems: The Ribosome Challenge

Lars V. Bock,[1] Sara Gabrielli,[1] Michal H. Kolář,[1,2] and Helmut Grubmüller[1]

[1]Theoretical and Computational Biophysics, Max Planck Institute for Multidisciplinary Sciences, Göttingen, Germany; email: hgrubmu@gwdg.de

[2]Department of Physical Chemistry, University of Chemistry and Technology, Prague, Czech Republic

Annu. Rev. Biophys. 2023. 52:15.1–15.30

The *Annual Review of Biophysics* is online at biophys.annualreviews.org

https://doi.org/10.1146/annurev-biophys-111622-091147

Keywords

computer simulations, molecular dynamics, cryogenic electron microscopy, cryo-EM, ribosome, translation, antibiotics

Abstract

Large biomolecular systems are at the heart of many essential cellular processes. The dynamics and energetics of an increasing number of these systems are being studied by computer simulations. Pushing the limits of length- and timescales that can be accessed by current hard- and software has expanded the ability to describe biomolecules at different levels of detail. We focus in this review on the ribosome, which exemplifies the close interplay between experiment and various simulation approaches, as a particularly challenging and prototypic nanomachine that is pivotal to cellular biology due to its central role in translation. We sketch widely used simulation methods and demonstrate how the combination of simulations and experiments advances our understanding of the function of the translation apparatus based on fundamental physics.

Contents

1. INTRODUCTION

From a theoretical physics perspective, biomolecules and biomolecular complexes are heterogeneously structured, strongly interacting many-body systems. In short, they are exceedingly complex. This structural complexity implies that the free-energy landscape arising from the large number of intra- and intermolecular interactions is high-dimensional and exhibits zillions of nearly iso-energetic (and, therefore, thermally accessible) minima, which are separated by a hierarchy of energy barriers (62). These properties of the underlying free-energy landscape govern the correspondingly complex internal motions of the biomolecule, which often cover a broad range of timescales, ranging from picoseconds to seconds or even hours (54, 217). It is this complexity on several levels that enables the biological function of the molecule. Indeed, a survey of small globular proteins suggests that combining knowledge of a protein's dynamics with knowledge of its structure significantly improves protein function prediction (81).

To cope with this complexity, a large variety of experimental techniques has been developed to study biomolecular dynamics and function. Each of these probes a particular subset of observables, often indirectly, such that obtaining a fully structural and causal explanation of protein function often remains challenging.

To connect experiments to protein function, and to explain functional processes from fundamental physics, molecular dynamics (MD) simulations (98, 196) have proven helpful and have over the past few decades provided a deeper understanding of increasingly complex systems. However, only recently—thanks to dramatic hardware, software, and methods advances—have larger biomolecular complexes consisting of millions of atoms, as well as functional processes on timescales longer than microseconds, also become accessible to computer simulations, thus addressing more and more problems in the life sciences.

In terms of system size, the first atomistic MD simulation containing one billion atoms was carried out recently for a simulation time of 1 ns (168). In terms of current simulation speed,

thanks to modern graphics processing units (GPUs), cheap current tabletop hardware delivers several hundreds of nanoseconds per day for moderately sized simulation systems (110), whereas the most recently developed specialized hardware is capable of performing 100 μs per day for systems containing one million atoms (179). As a result, an increasing number of biomolecular complexes and functions have become accessible to computer simulations over the past few years.

In this review, we highlight, from a computational perspective, the interplay between experiment and simulation for the prototypic example of the ribosome, a rather large RNA–protein complex that facilitates protein synthesis in the cell. Accordingly, this review does not aim to provide a comprehensive overview of the ribosome field. Instead, we refer the interested reader to recent excellent reviews on translation in prokaryotes (160, 161), ribosome structure (107), force spectroscopy with optical tweezers (30), cotranslational protein folding (123), nuclear magnetic resonance (NMR) of nascent chains (37), ribosomal frameshifting (158), and ribosome-targeting antibiotics (117).

Similarly, we are not able to comprehensively review the rapidly increasing literature on computational studies of the ribosome; we refer the reader to References 9, 24, 126, 167, and 192. Instead, we restrict our review to those simulation studies that serve to illustrate the above interplay by making direct contact with a particular type of experiment—either by providing structural or causal interpretations that would not be possible from the experiment alone or by attempting direct assessment of a particular simulation through experiments. Our main aim is to help bridge the gap between experimentalists and theoreticians in the ribosome field.

With this aim in mind, we first briefly sketch various simulation techniques relevant to studying the ribosome. We put particular emphasis on the multiscale nature of the problem and discuss various levels of spatial and temporal detail. Second, we illustrate by examples the interplay between computer simulation and different experimental approaches, with an emphasis on the mutual limitations and how they can be overcome. We structure this part according to which type of experiment the simulation links to. Each of these subsections are preceded by a brief sketch of each relevant experiment, followed by discussion of the relevant simulation studies.

2. STRATEGIES TO SIMULATE BIOMOLECULAR COMPLEXES LIKE THE RIBOSOME

In this review, we focus on biomolecular MD simulations, as opposed to other calculations such as electrostatics calculations (60). These simulations iteratively generate a time series of structures (snapshots) of the biomolecular complex under study, typically by numerically integrating Newton's laws of motion timestep by timestep for each single atom of the simulation system, which typically contains the biomolecular complex and part of its physiological environment. Taken together, these series of structures provide a molecular movie or trajectory. Ignoring the time information, the obtained set of structures may also approximate a statistical ensemble, from which thermodynamic quantities such as free energies or entropies can be derived.

The size of the ribosome is between 20 nm in bacteria and 30 nm in eukaryotic organisms, which translates into simulation systems of several millions of atoms (20, 53, 169). Functional processes of the ribosome cover timescales from picoseconds (peptide-bond formation) all the way to seconds [transfer RNA (tRNA) recruitment and processing or cotranslational folding].

The wide spatial and temporal ranges challenge current simulation techniques, mainly because of (*a*) the sheer size of the ribosome, (*b*) its complex chemical composition, and (*c*) the diverse rates of relevant motions and processes. As the saying goes, "there ain't no such thing as a free lunch," so obtaining more detailed or more accurate insights always requires computationally more demanding simulations. This trade-off between spatial resolution of the simulation and

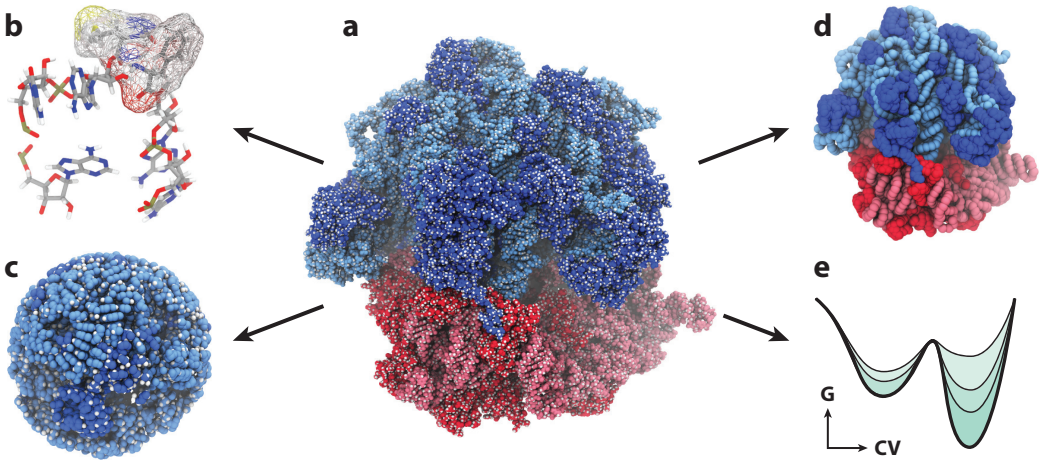

Figure 1

Overview of strategies for simulating the ribosome. (*a*) Atomistic model of the bacterial ribosome as an input for molecular dynamics (MD) simulations and other more simplified models. The large subunit is blue, and the small subunit is red. Darker colors are used for ribosomal proteins, and lighter colors are used for RNA. Hydrogen atoms are white. (*b*) A highly reduced single-conformation model represented by transfer RNAs (tRNAs) in A and P sites and the nucleotide A2602. The amino acid residues are highlighted by a mesh symbolizing a subatomic resolution of the typical calculation. (*c*) A dynamic reduced atomistic model constructed as a sphere around the peptidyl transferase center. (*d*) A coarse-grained model of the entire ribosome where each residue is represented by a single bead, as used in some MD simulations. (*e*) A simplified Gibbs free energy as a function of collective variable (CV) represents enhanced sampling methods, which can be applied to dynamic models of any resolution. The panels are not to scale.

simulation length or ensemble size requires, depending on the biological question at hand, different approaches and strategies (summarized in **Figure 1**), which we sketch briefly below.

2.1. Subatomic Level of Theory

The most accurate—and most expensive—simulation techniques consider the electronic degrees of freedom explicitly via quantum mechanics (QM) ab initio methods (116), semiempirical QM (SQM) methods (188), or Kohn-Sham density functional theory (DFT) (44). These methods are used for studying chemical reactions or processes involving electronic polarization or charge transfer. They have been heavily used to study smaller molecules and complexes, including biomolecules (67, 71, 94).

Because the ribosome is a catalyst, calculations at subatomic resolution have been mainly applied to study the peptide bond formation (peptidyl transfer between A-site and P-site tRNAs) (178, 200) or the release of the nascent chain (NC) from the ribosome (101). For instance, a combination of QM and DFT methods provided a computational support (200) for the currently accepted mechanism of the peptidyl transfer, in which an eight-membered ring transition state is formed involving an auxiliary water molecule (108, 173). In addition to the peptidyl transfer, the GTP hydrolysis during tRNA accommodation has been tackled by computations at the subatomic level (6–8, 11, 201). Recently, Mondal et al. (136) investigated the activation mechanisms of EF-G and EF-Tu with a particular focus on the allosteric contributions to GTP hydrolysis. According to their calculations, two different hydrolysis mechanisms involving either one (1W) or two (2W) molecules can account for the experimentally determined catalytic rates of the two GTPases. Moreover, their results suggested that both systems are activated by allosteric effects, in agreement with previous mutational studies (130).

Due to the enormous computational costs of quantum mechanical calculations for systems of this size, a single-conformer approach is usually adopted, i.e., no trajectory is generated. Because chemical reactions like the peptidyl transfer are fast, the slower conformational motions, conformational heterogeneity, and entropic contributions of the surroundings are thus often neglected. Thus, the results may differ depending on the conformation used. Structural details such as the orientation of a hydroxyl group or the position of a particular water molecule may notably affect results and conclusions. Therefore, the quality of the structural model is crucial.

In a notable exception to the single-conformer approach, Sharma et al. (178) used a series of short MD simulations with an empirical valence bond Hamiltonian to compare peptide bond formation in the ribosome and in solution. They suggested that the catalytic effect is largely due to reduction of solvation entropy.

Even at the single-conformer level, a full ribosome simulation system is too large for typical QM, SQM, or DFT calculations. These calculations are therefore carried out on reduced systems representing only a small portion of the ribosome, up to a few hundred atoms. Considering the local character of the chemical reactions of interest, the approach is often justified. If required, the effect of more distant parts of the system is included at a lower level of theory, e.g., molecular mechanics (MM). This type of method, known as QM/MM (177, 205), was used to study, e.g., keto-enol tautomerism in modified and unmodified nucleotides (78), its role in decoding (100, 170), and the mechanism of peptidyl transfer (91, 99, 111).

2.2. Atomic Resolution

Considerable insights into ribosomal function have been achieved at the atomistic simulation level, i.e., by studying the dynamics of individual atoms without explicit representation of electronic degrees of freedom. In our view, this level of model detail provides a particularly good trade-off between accuracy and computational cost for studying larger conformational motions. Atomistic MD simulation are well covered by several excellent textbooks (64, 193) and dedicated reviews (in the biomolecular context, see, e.g., 55, 97, 196).

At the level of all-atom MD (aaMD) simulations, the effect of the electronic degrees of freedom are captured via interatomic potentials (collectively referred to as a force field). Examples include harmonic approximations for bond stretching or bond angle bending, as usually used in aaMD simulations. Noncovalent interactions such as electrostatics, van der Waals attraction, and Pauli repulsion are described by Coulomb's law and Lennard-Jones potentials.

Calculating the interatomic forces resulting from these potentials for each time step of the simulation is the main computational bottleneck. Huge efforts have therefore been invested in developing and improving algorithms for the fast calculation of forces, particularly of Coulomb forces (105). As a result, up to 10^9 such integration steps can be carried out on high-performance hardware today within several weeks, depending on system size. With typical integration time steps between 2 and 4 fs, the currently accessible simulation times for the entire ribosome are several tens of microseconds.

Relatively accurate force fields have been developed for standard biomolecular chemical building blocks of ribosomes, amino acids, and nucleic acids (18, 125, 222). In addition, force fields have been developed for some noncanonical nucleotides of ribosomal RNA (rRNA) or tRNAs (2, 214). This is especially crucial for the investigation of certain ribosome parts or processes, which rely upon the chemically modified nucleotides. For instance, the decoding of certain codons is facilitated by modified nucleotides neighboring the anticodon on the tRNA (4).

For other chemically modified nucleotides or for small molecules such as ribosome-targeted antibiotics or fluorescent dyes, no force fields exist. The interaction parameters of these molecules

thus need to be either adapted from similar chemical compounds or derived from QM calculations of the molecule in question. This is usually a tedious procedure, although automatic or semiautomatic workflows do exist (92, 156). On the one hand, these workflows make the simulation protocols more accessible to nonexperts; on the other hand, the black-boxing of the parametrization procedure makes it prone to errors, especially in the absence of proper validation of the parameters. If possible, one should always validate these workflows against experiments.

For ribosome simulations, two force field families are commonly used, AMBER (125) and CHARMM (18, 222). Both force fields have a long history, and numerous studies have validated their use on smaller biomolecules and biomolecular complexes. Due to the ribosome size and computational demands, however, no rigorous assessment of the accuracy of these force fields at that level has been performed to date. Some studies have checked the robustness of their conclusions with respect to the choice of force field (53); however, this doubled the computational costs. As of now, therefore, the choice of force field is typically not governed by its (unknown) accuracy, but instead remains a subject of research group tradition, software availability, and the match with parametrization procedures for required nonstandard molecules.

The alert reader may have wondered why several millions of atoms are required for the simulation of a 2.5-MDa bacterial ribosome. In fact, most atoms are spent to explicitly include water molecules and salt ions, which strongly affect the energetics and internal motions of the ribosome. As a result, approximately 2 million atoms are required for bacterial (20), and approximately 2.5 million for eukaryotic (53), ribosomes. For systems of this size, and using a single GPU compute node, one can expect to simulate approximately 10 nanoseconds per day (110) or to spend three months per microsecond.

For this reason, whole-ribosome simulations are still rare. For example, aaMD simulations suggested an allosteric path from the surface of the bacterial ribosome to its interior (135). Because the allosteric signal transfers over large distances, it was necessary to simulate the entire ribosome. Likewise, due to the nonlocal character of the process, entire-ribosome aaMD simulations initiated from various functional substates were used to describe the energetics of tRNA translocation (20).

To reduce computational cost while keeping atomic resolution, many aaMD simulations have been performed involving only a part of the ribosome, e.g., only one of the two ribosomal subunits. Alternatively, simulation systems have been cut out from the ribosome such that they contain only atoms around the functional site of interest (**Figure 1**). Examples include the peptidyl transferase center (PTC) (13, 56, 87, 181, 201), the exit tunnel (29, 153, 223), and the decoding center on the small subunit (118, 119, 195). If the problem studied is well localized within the ribosome, then the system size may be reduced by up to 10-fold, thus allowing for longer simulation times and, accordingly, a more complete conformational ensemble. Commonly, the outermost residues are restrained by harmonic potentials to prevent the system from collapsing or evaporating (13, 87).

2.3. Coarse-Graining

To reduce computational demands, the dynamics of a system can be described at a more coarse-grained (CG) level, where the individual particles of the simulation system—or beads—represent not individual atoms, but rather groups of atoms or even residues (**Figure 1*d***). The main drawbacks of this approach, the lack of spatial detail and a less accurate description of intra- and intermolecular forces, are often outweighed by drastically improved conformational sampling. The main advantage of coarse-grained MD (cgMD) simulations of the ribosome is their computational efficiency, such that markedly longer time scales of up to seconds can be accessed (133).

Accordingly, cgMD simulations are used to study processes that are so slow that they are inaccessible to aaMD simulations. As with aaMD simulations, cgMD simulations can be used to

study nonequilibrium processes. For instance, a CG model, where each NC residue was modeled as a single bead centered on the C_α atom, was carried out to study cotranslational folding of the protein G domain and β-galactosidase domain in the presence of the trigger factor (148).

CG models may be combined with Langevin dynamics, which includes a stochastic term to account for thermal fluctuations. For instance, Bui & Hoang (27–29) studied the folding and escape of NCs under various conditions. Their cgMD simulations suggested escape times on a submillisecond timescale. A more extensive cgMD simulation, however, suggested that the escape times vary broadly and are mostly determined by the presence of charged residues in the NC sequence (146). cgMD simulations of co- and posttranslational protein folding predict formation of near-native entangled conformational states, which are proposed to bypass the proteostasis network (144). The observed kinetically trapped entangled conformations are in qualitative agreement with limited proteolysis mass spectrometry data, suggesting that nonfunctional conformations can prevail in the cell for long time periods.

There is no unique and widely accepted setup of cgMD simulations. Instead, in each study, the model is tailored toward its specific requirements. Still, there are some common practices that guide the model building in two main directions. In the bottom-up or physics-based approach, the parametrization of interparticle interactions is based on thermodynamic properties, which makes the parameters somewhat transferable between various biomolecules. In the top-down or structure-based approach, the interaction potentials are derived empirically from existing structural data and are thus system specific. In top-down approaches, the tunable parameters might be at risk of overfitting. Thus, comparing to experimental data, e.g., by cross-validation against independent data, is particularly crucial in this case.

A widely used bottom-up CG model is the MARTINI force field (132). It was originally derived for cgMD simulations of biological membranes (131). Later, it was extended to also include proteins and nucleic acids, which made it possible to simulate the ribosome (194). In the MARTINI force field, beads represent groups of atoms. Its implementation in popular MD simulation software (49, 155) makes its use straightforward.

The parametrization of the MARTINI force field is based on free energies. The loss of entropy caused by merging atoms into beads is compensated for by reduced enthalpies. This approach is valid only at a specific temperature, however, which has to be taken into account when considering the temperature dependence of processes (131, 132). In addition, coarse-graining generally leads to a smoother free-energy landscape compared to atomistic simulations and, therefore, artificially accelerated dynamics, which needs to be corrected for.

MARTINI cgMD simulations were used, e.g., to study translocon-mediated integration of NCs into the membrane. The simulations yielded parameters for an even coarser model, where a single bead represented three amino acid residues of the NC (142, 143), allowing the developers to study processes at the timescale of minutes. The simulations provided a picture consistent with experimental efficiencies of polypeptide integration into the membrane, including sequence-specific variations (143). This study also suggested ways in which NC processing can regulate ribosomal frameshifting in some viruses (34, 77).

Top-down structure-based models, often referred to as Gō models (70), are derived from a known low free-energy structure of a biomolecule. For each structure, the force fields are deliberately constructed so as to reproduce the structure as their lowest free-energy minimum, e.g., by including each native contact, and only the native contact, as a favorable interaction. Such models allow one to observe large conformational transitions at a highly reduced computational cost. Important limitations result from this construction, which only ensures that the free-energy minimum region is described properly but does not aim to accurately describe the remaining vast conformational free-energy landscape. In particular, the solvent is modeled implicitly, no

explicit electrostatics are generally taken into account, and contacts of metastable conformations or transition states are generally not described properly. Therefore, the obtained pathways are often sterically plausible but might not be the energetically most favorable ones. Recently, Wang et al. (202) introduced a structure-based model that takes electrostatics and explicit ions into account to study the effects of ion concentration on tRNA dynamics.

Numerous structure-based simulations of the ribosome have been prepared with the SMOG modeling package (147), as extensively reviewed by Levi et al. (113). For instance, structure-based CG models have been used to study NC dynamics (27, 144, 146, 189).

2.4. Enhanced Sampling Methods

The free-energy landscape that governs the conformational and functional dynamics of biomolecules is very complex and rugged, with an astronomical number of almost iso-energetic minima. These are connected by a hierarchy made up of a broad range of free-energy barriers that give rise to a correspondingly broad range of kinetic rates (62, 197). Because the probability of visiting a conformational state of energy E at temperature T is proportional to its Boltzmann factor $\exp(-E/k_{\mathrm{B}}T)$, where k_{B} is the Boltzmann constant, high-energy barriers are rarely overcome in unbiased simulations. As a result, conformational sampling by unbiased MD simulations is somewhat limited, essentially to the region around the starting conformation surrounded by high free-energy barriers.

Over the past few decades, specialized algorithms to overcome this limitation and to render rare events more likely to occur in MD simulations have been developed and greatly improved. These are collectively termed enhanced sampling methods and include, among many others, replica exchange simulations, umbrella sampling, conformational flooding, metadynamics, and steered MD. We refer the reader to excellent recent reviews (17, 90, 216) and simply sketch the main idea: The crossing of barriers is accelerated by a carefully crafted and controlled biasing potential, which modifies the genuine Hamiltonian of the system. As a result, a larger conformational space is explored within a given time span than in unbiased MD simulations. Although the thermodynamics of the system is artificially perturbed by these enhanced sampling methods, it can in most cases be accurately recovered—sometimes even together with the kinetics—by reweighing the obtained ensemble by the (known) Boltzmann factor of the biasing potential.

Enhanced-sampling MD was used, for instance, in a study of the translational arrest of the human XBP1 peptide (53). The distance between N-terminal peptide residue and solvent outside the ribosome was used as the biasing collective variable for the adiabatic bias MD. Vu et al. (199) used umbrella sampling MD simulations along the curved path through the exit tunnel to study water ordering within the tunnel vestibule. They argued that the ordering modulates the cotranslation protein folding.

3. COMPLEMENTING EXPERIMENTAL METHODS WITH SIMULATIONS

In this section, we discuss the interplay between simulations of and experiments on complex systems, focusing on the ribosome as an example. Simulations can be instrumental in the interpretation of experimental data and give rise to new hypotheses that can then be tested in experiments. We give examples of studies at the interface of simulation and experiment, sorted according to the type of experiment.

3.1. Cryogenic Electron Microscopy and X-Ray Crystallography

All molecular simulations of the ribosome and its components require a starting conformation based on experimentally obtained structural information. In most cases, the structural information

that is used is obtained from X-ray crystallography or cryogenic electron microscopy (cryo-EM) experiments (107). MD simulations can be used to refine atomistic models against cryo-EM maps. In fact, chemically diverse ribosomes consisting of proteins and RNA served as test cases for the development of MD-driven cryo-EM refinement methods (88, 102, 191).

Structures of short-lived conformational or compositional states are often obtained by trapping the complex in that state. Trapping can be achieved, e.g., by bound antibiotics that hinder conformational changes or the binding and unbinding of factors (59, 66, 164, 174, 183). Furthermore, chemical modification of reactants can prevent them from reacting, thereby trapping the complex in a state before the reaction. After the aminoacyl-tRNA accommodates into the A site, peptide-bond formation occurs rapidly. Using modified tRNAs, in which the ester linkage between the amino acid and A76 was replaced by an amide, allowed the resolution of structures mimicking the prepeptidyl-transfer state (154, 198). Nonhydrolyzable GTP analogs are often used to trap the complex in a prehydrolysis state. In addition, mutations that prevent chemical or conformational changes, e.g., mutations that render the elongation factors EF-Tu or EF-G incapable of GTP hydrolysis, are used to trap ribosome complexes (47, 48, 83).

From the simulation perspective, structures of these trapped states open up a promising route to study functional conformational motions that are experimentally inaccessible. Removing the trap in the simulations, e.g., the antibiotic (10, 13, 182, 204), allows the exploration of biologically relevant conformations that are currently not accessible experimentally. For example, the antibiotic kirromycin binds to EF-Tu and sterically prevents a conformational change of EF-Tu. Consequently, the dissociation of EF-Tu from the ribosome during decoding cannot occur (163). This effect enabled the determination of the first cryo-EM structure of ribosome–EF-Tu complex (183). aaMD simulations begun after the removal of kirromycin showed a rapid closing of the interface between domains 1 and 3, which is otherwise sterically blocked by the bound antibiotic (204). This closing is coupled to an opening of the interface formed by domains 1 and 2 that binds the CCA-tail of the tRNA and is therefore suggested to be a primary step in tRNA dissociation.

A cryo-EM map of the stalling nascent peptide VemP showed two conformations of rRNA nucleotide U2506 located in the PTC, whereas for the rest of the complex, no conformational substates were resolved (185). Two sets of MD simulations were initiated from the cryo-EM structures that only differed in the U2506 conformation, thereby generating two structural ensembles (106). Interestingly, the two average structures of each of the sets showed deviations from the cryo-EM structure up to 2 nm from the PTC. In contrast, the structure averaged over the two ensembles showed much smaller deviations, suggesting that, using MD simulations, subensembles can be distinguished and described that cannot be resolved with cryo-EM.

Another simulation-based approach to interpreting cryo-EM data, in this case the 2D images, was presented recently by Giraldo-Barreto et al. (69). They developed a Bayesian approach to obtain the free-energy landscape along a path in configuration space from a set of cryo-EM images. The path, which is a necessary input for this method, can be obtained from steered MD simulations, as demonstrated for the TMEM16F ion channel (69). For the ribosome, with this Bayesian approach of combining MD simulations with cryo-EM images, one could obtain, for example, free-energy profiles of decoding or tRNA translocation. A limitation of this approach is that a free-energy estimate of intermediate conformations along the path can only be obtained if there is a sufficient number of images corresponding to each intermediate. Specifically, for transition states of high free energy, this might require an amount of images that is experimentally not feasible.

Cryo-EM requires high vacuum, which makes it impossible to study biomolecules in liquid solutions. To preserve biomolecules in the hydrated state that can be imaged by electron

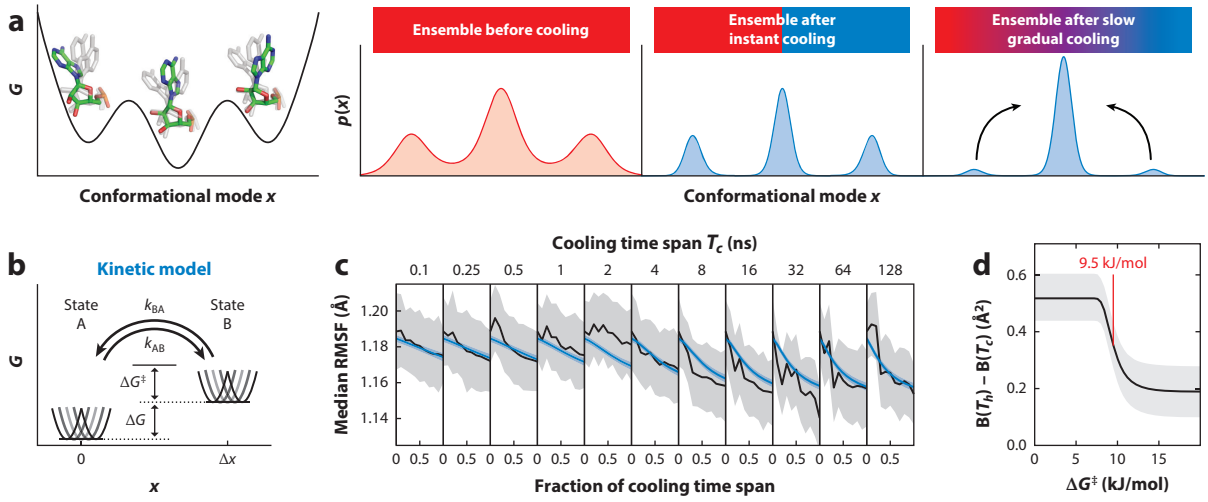

Figure 2

Atomistic simulation of cryogenic electron microscopy (cryo-EM) cooling and its effect on structural ensembles. (*a*) Schematic of a free-energy landscape along a conformational mode (*left*) and probability densities of structural ensembles (from left to right) before cooling, after instant cooling, and after slow cooling. (*b*) Kinetic two-state model of the cooling process. (*c*) The median root mean square fluctuations (RMSF), i.e., the width of the distribution of atom positions, is shown for an ensemble of ribosome structure. The RMSF was obtained from temperature-quench molecular dynamics (MD) simulations at different cooling times (*black*) and a kinetic model (*blue*). (*d*) Difference between B-factors at the temperatures before cooling (T_b) and after cooling (T_c) calculated from the kinetic model as a function of barrier height $\Delta G^{\ddagger}$. The temperature drop was estimated from a continuum model. Figure adapted with permission from Reference 23.

microscopes, the solution containing the biomolecules is first spread into a thin film and then plunged into a cryogenic liquid, e.g., liquid ethane kept at 90 K. The rapid cooling achieved by plunge-freezing results in biomolecules embedded in vitreous ice. The question is to what extent this shock-frozen ensemble represents the physiological ensemble at ambient temperatures (**Figure 2*a***). A recent study addressed this question by combining atomistic MD simulations of the ribosome–EF-Tu complex with continuum models and kinetic models (23) (**Figure 2*b–d***). Three effects resulting in differences between ensembles before and after cooling were quantified. Two effects were independent of the rate of the temperature drop: thermal contraction of the biomolecules and equilibration within local potential wells. The third effect, which depends on the temperature drop rate, is the equilibration into lower free-energy conformations via overcoming the barriers that separate the conformations. Rapid cooling kinetically traps the biomolecules in the conformations that they had before cooling, resulting in a cooled ensemble that is similar to the ensemble before cooling. Slower cooling gives the biomolecule more time to equilibrate into lower free-energy minima and results in more homogeneous ensembles. For the temperature drops estimated for experimental conditions, barrier heights below approximately 10 kJ/mol were found to be overcome (23), thus modifying the ensemble (**Figure 2*d***).

3.2. Kinetic Measurements

In kinetic measurements, the change of observables, e.g., the fluorescence of introduced dyes or the concentrations of reactants and products, is measured over time, starting from a state out of equilibrium. These measurements allow the determination of interconversion rates between different discrete states. Combining the measurements of several observables allows the determination of complete kinetic mechanisms (14, 151). The internal conformational motions of biomolecules are

governed by diffusion in a free-energy landscape, and individual states are separated by free-energy barriers.

To connect the free-energy landscapes obtained from simulations or experiments with rates obtained from kinetic measurements, Whitford et al. (209) extracted diffusion constants of functionally relevant collective rearrangements from aaMD simulations, e.g., for tRNA motion in pretranslocation states. Combining the diffusion constant with kinetic measurements, they estimated upper bounds for free-energy barriers. Using a similar approach, Yang et al. (215) estimated the diffusion constant for a tRNA motion during tRNA elbow accommodation from aaMD and structure-based cgMD simulations. In the aaMD simulations, they found a strong dependence of the diffusion constant on the position of the tRNA along the accommodation reaction coordinate. This dependence was absent in the cgMD simulations, suggesting that the position dependence arises from electrostatic interactions with the solvent, which were not taken into account in the cgMD simulations. This notion was supported by the observation that the number of contacts with the ribosome anticorrelated with the diffusion constant. Hassan et al. (79) provided a detailed review of computational and theoretical approaches to describing the energetics of subunit rotation.

Bock et al. (20) investigated the dynamics and energetics of tRNA translocation in the absence of the elongation factor EF-G. aaMD simulations were begun from X-ray structures refined against cryo-EM density maps of ribosomes in 13 intermediate translocation states (57). For the large-scale conformational motions of the tRNAs and the L1 stalk, as well as 30S head and body rotations, the intrinsic transition rates were estimated from the overlap between states. The estimated rates suggested that the rates of tRNA motion are slowest and, due to the mutual coupling of motions, also rate limiting for spontaneous tRNA translocation. MD simulations suggested that the fast rates for intersubunit rotation are facilitated by a dynamically adapting network of intersubunit contacts (21). It was argued that conformational flexibility determines the thermodynamic balance of the rotated versus the unrotated state (63). Furthermore, simulations were used to optimize structural metrics that can identify the free-energy barrier of subunit rotation (115).

For conformational changes involving many components of a large complex, simulations help to identify rate-limiting motions. During decoding in the ribosome, the tRNA delivered as a part of the ternary complex undergoes large conformational changes to reach the GTPase-activated state. In aaMD simulations of the isolated ternary complex, the tRNA was found to interconvert between different conformations found in cryo-EM structures of the ribosome complex on microsecond timescales (58). Since GTPase activation takes milliseconds, the conformational changes of the tRNA do not appear to be rate limiting for the GTPase activation.

Cryo-EM and X-ray crystallography provide information on conformations occupying local free-energy minima crucial for the thermodynamics of a biomolecules. However, the kinetics are largely determined by high-energy transition states. MD simulations with additional biasing potentials can be used to drive a biomolecule between conformational states, thus predicting transition state conformations, and to identify contacts that shape the barrier. These contacts can then be tested via a combination of mutagenesis and kinetic experiments. For the ribosome, Sanbonmatsu et al. (169) pioneered this approach by driving tRNA accommodation into the ribosomal A site. With structure-based cgMD simulations, known tRNA translocation intermediates were successfully recovered, and new ones were postulated (140).

Ge et al. (68) combined kinetic measurements, mutagenesis, and MD simulations to uncover electrostatic interactions between the ribosomal stalk protein L7/L12 and the initiation factor IF2, which is crucial for subunit association. The simulations predicted that pairs of L7/L12 and IF2 residues would form tight salt bridges. Mutations of single interacting residues showed large defects in subunit association, which were restored with charge-reversing mutations of two interacting residues, thereby confirming the predictions.

During NC elongation, stretches of positively charged amino acids can dramatically decrease translation rates (124). Leininger et al. (111) combined cgMD, aaMD, and QM/MM simulations of charged and uncharged NCs in the exit tunnel and suggested that the interaction of positive NC residues with the tunnel walls resulted in a force acting on the amino acid residue attached to the P-site tRNA. Due to the force, the residue is pulled away from the amino acid attached to the A-site tRNA, thereby increasing the free-energy barrier of peptide bond formation. The predictions of the simulations were found to agree with ribosome profiling data.

3.3. Force Spectroscopy

Force spectroscopy with optical tweezers is routinely used to study cotranslational folding of proteins (30), allowing researchers to determine the sequence of folding events and the corresponding rates (121, 212). Several studies combined optical tweezers experiments with MD simulations to study cotranslational folding (213) and messenger RNA (mRNA) secondary structure elements that slow down translation (86, 208, 221).

Wruck et al. (213) measured folding and unfolding of the small protein domain ADR1a inside and outside of the ribosomal tunnel using an assay combining optical tweezers with single-molecule Förster resonance energy transfer (FRET). When the protein domain was connected to the P-site tRNA with a short linker, the domain resided inside the tunnel, while with a longer linker, the domain emerged from the tunnel. Inside the tunnel, the domain was found to fold more rapidly, and the folded state was found to be more stable, compared to the domain outside of the tunnel, showing that the environment inside the tunnel can modulate folding. These observations were qualitatively reproduced in cgMD simulation only when electrostatic interactions between ADR1a and the ribosome were included. Umbrella sampling simulations were used to estimate the folding free energy and a free-energy barrier associated with the folding. In the simulations, the electrostatic protein–tunnel interactions contributed to a lower barrier. These results suggest that excluded volume effects are not sufficient to account for the modulated folding and that the interplay between the tunnel and the nascent peptide has to be taken into account. A similar conclusion about the decisive role of the exit tunnel in cotranslational folding was drawn from MD simulations of VemP in the ribosome and in solutions, accompanied by circular dichroism spectroscopy (106).

Force-sensitive arrest peptides, e.g., SecM or VemP, are short amino acid sequences that, during their synthesis, stall ribosomal translation (211). Optical tweezers experiments established that forces applied to the N terminus of the peptide can release the stalling (72). To obtain a molecular picture of how a force induces the release of stalling, Zimmer et al. (223) carried out nonequilibrium atomistic MD simulations begun from cryo-EM structures of stalled SecM and VemP peptides (185, 218). To mimic the force-ramping protocols used in optical tweezers experiments, they applied a force ramp to the N terminus, albeit with faster rates than in the experiments due to the limited timescales accessible by the simulations (223). However, the sequence of SecM conformational changes was consistent over two orders of magnitude of the force-ramping rate, suggesting that it is somewhat independent of the pulling rate. Furthermore, simulations of SecM mutants reproduced their effects on stalling efficiencies obtained from experiments. The results allowed Zimmer et al. to distinguish two groups of the amino acids crucial for stalling, one that induces stalling due to specific interaction with the ribosome at the PTC and another that stabilizes the conformation of the overall peptide and resists external forces.

Using small beads with a high refractive index and low light absorption, optical tweezers can reach temporal and spatial resolutions on the order of microseconds and nanometers (186). Such high temporal resolutions overlap with the timescales accessible by aaMD simulations. Recently,

atomic force microscopy (AFM) of a small ligand–protein system and aaMD simulations reached a high overlap of timescales (157). The rupture forces obtained from the MD simulations agreed nicely with the measured values; thus, it is likely that a more direct comparison of experiments and simulations can also be achieved for larger systems like the ribosome.

Interestingly, imaging with high-speed AFM (HS-AFM) reaches subsecond time resolutions sufficient to visualize structural dynamics of the ribosome, as shown by a recent visualization of P-stalk dynamics (89). In addition to the observation of structural dynamics, HS-AFM can also monitor spatial distributions of biomolecules. Currently, the timescales achievable by HS-AFM are outside of the timescales reached by aaMD simulations. However, the combination of experimental results with CG simulations has the potential to provide important information on the dynamics of the translation machinery.

3.4. Arrest-Peptide Force-Measurement Assays

The cotranslational folding of a protein (domain) close to the ribosome can result in a pulling force on the NC. The translational arrest caused by some arrest peptides (AP), e.g., SecM, can be released by a force applied to the N terminus (72). This force-induced release is used in AP force-measurement experiments to monitor force generated by cotranslational folding of proteins (72, 189). To that end, the mRNAs encoding the protein sequence followed by a linker and the AP sequence are translated by the ribosome. The yield of full-length protein that escapes the arrest serves as a proxy for the pulling force exerted on the NC by the protein as it folds. Varying the length of the linker allows one to obtain a force profile and to identify when the force-generating folding events occur during translation.

Tian et al. (189) used cgMD simulations of the titin domain I27 in the tunnel with different linker lengths and calculated the forces acting on the NC. In their simulations, they used one bead per amino acid and three beads per nucleotide. Peptide–peptide interactions were given by a structure-based model, and peptide–ribosome interactions were set to be purely repulsive. The obtained forces were combined with the previously determined relationship between the arrest escape rate and the force acting on the NC (72) to estimate the yield of full-length protein. The resulting yields as a function of linker length agreed well with the measured yields, suggesting that the simulations are able to predict the correct forces and the correct linker lengths at which folding occurs.

3.5. Förster Resonance Energy Transfer

In FRET experiments, the distance-dependent efficiency E of an energy transfer between a donor and an acceptor dye, $E = 1/[1 + (r/R_0)^6]$, is used as a molecular ruler (184) to probe nanometer distances in biomolecular systems (61). In this case, r is the distance between the two dyes, and R_0 is the so-called Förster radius, which, crucially, depends on the (properly averaged) mutual orientation of the dyes, quantified by a orientation factor κ^2. For freely diffusing dyes with uniform and uncorrelated orientational distributions, $\kappa^2 = 2/3$, such that the distance r can readily be calculated from the measured efficiency (184).

Both from an experimental and from a simulation perspective, experiments on single molecules [single-molecule FRET (smFRET)] are particularly informative, as they monitor distance fluctuations with millisecond time resolution and thus provide kinetic information on functional molecular processes. For this reason, smFRET has been widely used to investigate the structure and dynamics of the ribosome (15, 138, 162). To probe internal motions of the ribosome, the donor and acceptor dyes are chemically attached to well-defined and carefully chosen positions within the ribosome; thus, the observed efficiency fluctuations reflect well-defined conformational

motions. Using several different position pairs, these motions can be triangulated throughout the ribosome (95).

However, more often than not, the dyes interact with the ribosome or are even buried inside it, such that their orientational dynamics is severely hindered. As a result, κ^2 is no longer 2/3, and therefore, the quantitative reconstruction of distances and distance distributions from the FRET efficiencies becomes challenging.

In this case, aaMD simulations of the dye orientational dynamics and its close environment can help by providing statistics from which κ^2 can be readily calculated (82). These MD simulations were used, e.g., to probe the experimentally inaccessible mutual dye orientations during conformational motions in a polyproline chain. Instantaneous transfer rate coefficients were then calculated from the time-dependent mutual orientations. Monte Carlo simulations of the FRET kinetics served to collect photon statistics and, thus, compute the efficiency distributions. The good agreement between computed distributions and experimental efficiencies showed that this combined aaMD/smFRET approach indeed yields markedly improved distance estimates. This idea has recently been refined along several lines of research, e.g., for improved sampling (96), for a more realistic description of the dye's photophysics (187), and to account for the proper statistics for single-photon counting (73, 175).

A further limitation of FRET experiments stems from an often suboptimal positioning of the FRET probes. Since the conformational transitions are monitored only by the rather limited information provided by the distance between the two dyes, relevant conformational states or transitions may be overlooked. Indeed, different accessible states can easily generate indistinguishable FRET signals. Using structure-based Gō-type simulations, Levi et al. (114) identified hidden conformations of A-site and P-site tRNAs during the formation of the P/E hybrid state. In particular, while a study from Munro et al. (137) identified three states, the simulations suggested that those signals could originate from up to seven combinations of A-site and P-site tRNA conformations.

Different labeling strategies sometimes yield seemingly contradictory results. This was the case for two experiments independently designed to monitor the spontaneous rotation of the 30S subunit (45, 134). However, based on structure-based CG models, the conflicting observations were rationalized by taking intrasubunit flexibility into account (112). Moreover, by comparing the distances probed by smFRET experiments to collective variables that typically describe subunit rotation, Levi et al. (114) identified those distances that are most responsive to subunit rotation. The combination of FRET measurements with MD simulations has also been used for cross-validation (210) and to investigate the structural origins of the observed FRET efficiencies (1, 103, 145, 190).

These examples show how MD simulations are used today not only to complement smFRET efficiency distributions with structural interpretations, but also as a tool to design and enhance experiments, e.g., by optimizing dye positions.

3.6. Nuclear Magnetic Resonance

Thanks to recent developments, it is now possible to use NMR to study biomolecular complexes with a molecular weight in the MDa range (5, 176, 203). These new capabilities integrate structural data from cryo-EM and X-ray crystallography with atomic-resolution information on ribosome motions, including the most flexible regions on the ribosome's surface. Indeed, numerous NMR studies, which have been recently reviewed (37), have focused on the structure and dynamics of ribosome-bound NC complexes. The information from solution-state NMR experiments is, however, often limited to specific regions of the ribosome: In contrast to the regions on the surface, the

core of the system tumbles too slowly to be observed. Moreover, from NMR data, it is extremely challenging to solve the structural ensemble sampled by large molecules. MD simulations combined with NMR enable more detailed insight into the dynamical processes of interest. Using the structural information from NMR experiments to introduce restraints in MD simulations (120, 159) ensures a more realistic conformational sampling. In addition, enhanced sampling techniques can be used in combination with the restraints to accelerate crossing of high free-energy barriers. For example, Camilloni et al. (33) proposed the replica-averaged metadynamics scheme, where experimental restraints are combined with metadynamics and replica exchange.

Combined approaches were applied in studies on the trigger factor (TF) in solution and in complex with the ribosome (52, 148, 166). The TF is a bacterial chaperone that binds to the ribosome during translation and interacts with the NCs emerging from the tunnel exit. Since the NCs that bind to the TF are highly dynamic, obtaining detailed structural information on the interaction between the TF and its substrates is challenging. Still, recent advances in NMR spectroscopy and isotope labeling enabled the study of the binding of alkaline phosphatase to the TF in solution (165).

Simulations by Deeng et al. (52) integrated the NMR results obtained for the TF in solution by Saio et al. (165) and provided insight into the interaction between the NC and the TF when the TF was bound to the ribosome. In the study, the TF, the NC, and ribosomal proteins were modeled atomistically, while the remaining parts of the system were CG (52). In terms of the interactions of the NC with the C-terminal and head domain of the TF, the simulations agreed well with the NMR results. However, marked differences were observed within the ribosome binding domain (RBD). In particular, the simulations identified hydrophobic interactions between the RBD and the NC, which were not seen in the NMR experiment. Deeng et al. attributed this difference between the simulations of the ribosome-bound complex and the NMR experiments on the TF in solution to a rearrangement of the RBD. Indeed, their cryo-EM experiments showed that the hydrophobic surface of the RBD is exposed toward the NC upon binding to the ribosome.

O'Brien et al. (148) tuned the interactions between the TF and the ribosome in their simulations so that they could reproduce experimental dissociation constants between both the TF and the ribosome and the TF and the NC. They performed cgMD simulations to investigate how the TF alters the cotranslational folding of nascent proteins. Although the presence of the TF did not affect the folding properties observed for a small protein, it was observed that, at a NC length where the N-terminal domain of a larger β-galactosidase is completely outside the exit tunnel, the TF decreased the population of the domains' folded state. Based on their simulations, they suggested that the origins of the decrease in folded population are kinetic and not thermodynamic, in agreement with a previous experimental study (3). In addition, they identified three molecular mechanisms generating the kinetic control of the process. When studying the oligomerization of TF factor in solution, MD simulations have been used as a tool in structure refinement. For example, Saio et al. (166) employed MD simulations to refine structures of the TF dimer using distance restraints based on nuclear Overhouser effect (NOE) measurements, dihedral-angle restraints, and hydrogen-bond restraints.

NMR experiments combined with MD simulations were used to study NCs and cotranslational folding. Cassaignau et al. (35) used NMR spectroscopy and cgMD simulations to probe the interaction between unfolded NCs and the ribosome surface. Starting from experimental estimates of the binding frequency of the NC to the ribosome, they used NMR data to calibrate the strength of electrostatic interactions in their CG model. The MD simulations allowed them to characterize the structural ensemble of the NC and explore the interactions between the NC and the ribosome surface. In a similar study, a structural ensemble of the NC was obtained by using measured chemical shifts as restraints in replica-averaged metadynamics MD simulations (31).

Deckert et al. (50, 51) investigated how NCs interact with the ribosomal surface before cotranslational folding was initiated. For this purpose, they examined the NC of the intrinsically disordered protein α-synuclein (αSyn). Their cgMD simulations served to provide an explanation for the broadening and decrease in intensity of the NMR resonances of αSyn in the presence of the ribosome and TF. More recently, they systematically investigated the effects of electrostatics, aromatic groups, and the length of the NC, integrating the data with restrained atomistic simulations (50) (**Figure 3**). Structural information on the orientation of the NH covalent bonds in the NC was obtained from NMR residual dipolar couplings (RDC) for the backbone amide resonances. The RDCs were used as restraints in aaMD simulations, following the well-tempered bias-exchange metadynamics protocol. The simulations displayed the orientations preferred by the NC and suggested that the residues involved in the interactions with the ribosome are also involved in recruiting the TF. Interestingly, these results suggest that the ribosome might act as a holdase by reducing NC mobility and preventing misfolding until the handover to the TF.

One of the bigger challenges of cotranslational folding studies stems from the fact that the volume of the conformational space explored by the NC increases with increasing chain length (43). As a consequence, the folding free-energy landscape consists of a series of nested landscapes, each of which is associated with a different NC length. As the length increases, the energy landscape, as well as the conformational dynamics that it governs, becomes increasingly complex. For this reason, probing and sampling the cotranslational folding landscape experimentally is particularly challenging, as extensively reviewed by Waudby et al. (206).

One strategy to reproduce the states of the folding pathway during translation consists in designing intermediates of the pathway by truncating the full-length chain (the FLN5 domain from filamin) at different distances from the C terminus (207). The folding pathway and kinetics were characterized by systematic analyses of these stalled NCs. To investigate how the truncation position affects the chemical shift perturbations, Waudby et al. (207) observed that the variant obtained by truncating at a distance of six residues from the C terminus displayed an additional set of native-like resonances. Enhanced sampling MD simulations of this variant elucidated the structural rearrangements of the NC in the folding pathway. In particular, this study highlighted the key role of proline isomerization during the process. In addition, metadynamics simulations of a structure-based model provided an estimate for the misfolding probability. Interestingly, Waudby et al. observed that this probability decreased drastically when the proline isomerization was accelerated by dedicated enzymes. Recently, two previously unobserved cotranslational folding intermediates of the FLN5 domain (I_1 and I_2) have been detected using ^{19}F NMR (38). Structural ensembles generated by structure-based, cgMD, and electron-density-guided atomistic MD simulations (88) qualitatively agreed with the NMR data of I_1 and I_2. Based on the simulations, two residues of the NC were predicted to strongly interact with the ribosome stabilizing the intermediates. The prediction was tested by mutation of the two residues. In agreement with the predictions, ^{19}F NMR spectra displayed a shift of populations from the intermediates to the native structure in the presence of the mutations. However, the result also suggests that the interactions predicted by cgMD only partially describe the interactions with the ribosome in the intermediate states and that a further model refinement is required.

An MD simulation study of cotranslational folding suggested that long-range contacts within the exit tunnel are necessary for initiating the folding of the NC (149). In agreement with NMR data, folding at the interface of the exit port was observed for two of the tested NCs (32). For a large set of tertiary structure motifs, the CG model correctly predicted their ability to sterically fit within the exit tunnel.

Thanks to recent advances, electron paramagnetic resonance (EPR) has also been used to investigate rRNA and ribosome interactions (127–129). A recent study by Fries et al. (65) used MD

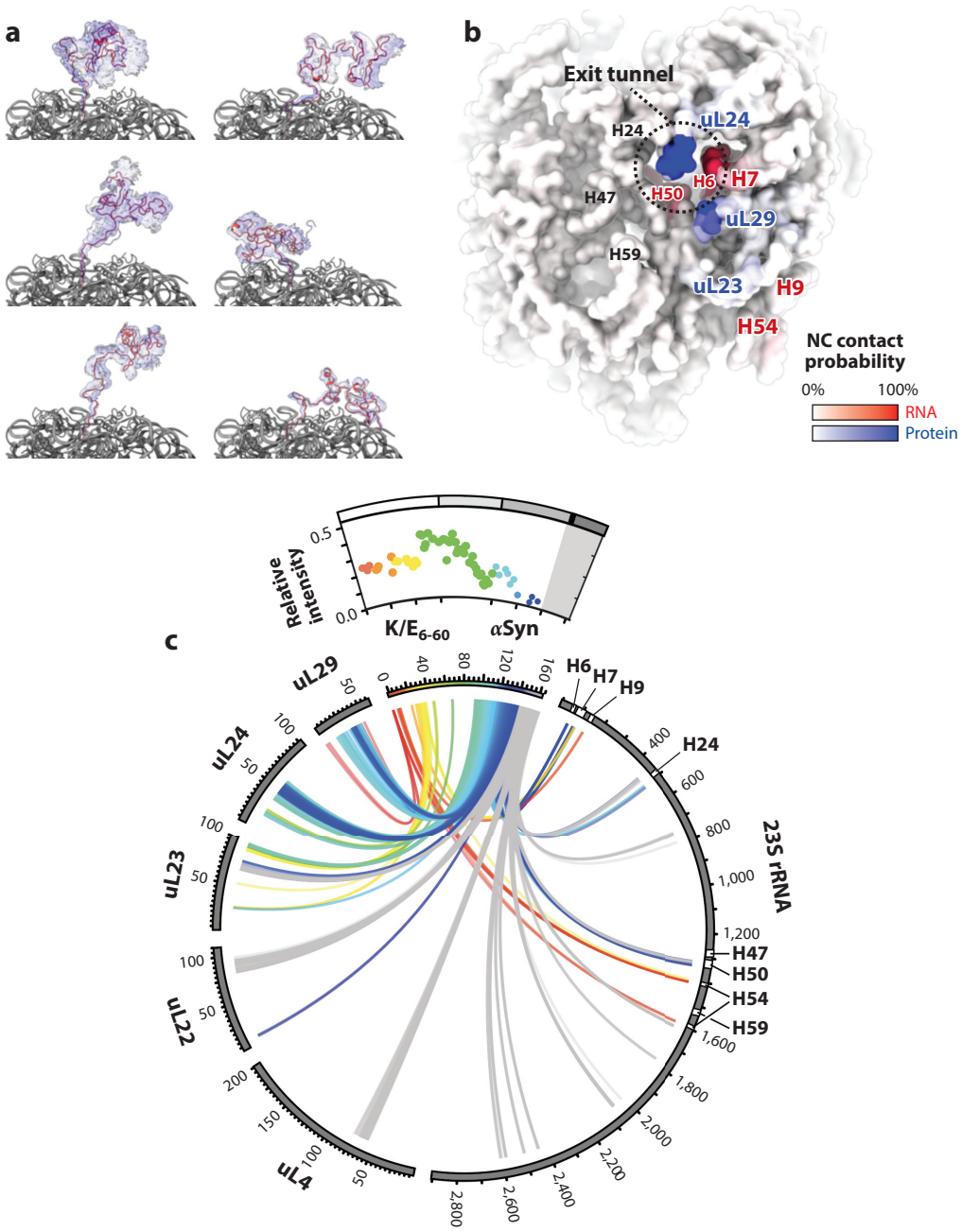

Figure 3

Atomistic simulations of the α-synuclein (αSyn) nascent chain (NC) complementing nuclear magnetic resonance (NMR) experiments. Ribosome atoms were kept fixed during the simulation, apart from those within flexible loops and disordered tails of ribosomal proteins that line the exit tunnel and the ribosome surface. Residual dipolar couplings (RDCs) were used as restraints, and the well-tempered bias-exchange metadynamics protocol was applied. (*a*) Structures of the six most-sampled conformations. (*b*) Surface representation displaying the NC interaction sites on the ribosome. The sites are colored according to binding frequency with ribosomal RNA (rRNA) (*red*) and ribosomal proteins (*blue*). (*c*) Interactions between the NC and the ribosome, colored by primary sequence. The NC relative cross-peak intensities from NMR experiments are shown above the circular plot. Figure adapted from Reference 50.

simulations as an aid to examine conformational changes of the eukaryotic ribosome-associated complex upon ribosome binding. Future developments in the EPR field might increasingly utilize MD simulations in a manner similar to what is already routine for NMR today.

3.7. Frameshift Assays

During elongation, the ribosome decodes the mRNA one nucleotide triplet (codon) at a time with the help of tRNAs, each of which carry a specific amino acid. The interaction of three tRNA nucleotides (anticodon) with the codon nucleotides determines if the amino acid is added to the NC. After peptide bond formation, the ribosome translocates along the mRNA by three nucleotides. Generally, the reading frame is fixed during initiation and maintained throughout elongation such that spontaneous frameshifting is extremely rare (109). However, certain mRNA sequences have evolved to result in high frameshift efficiencies, i.e., the share of peptides that are encoded by the shifted reading frame. The most common type of such programmed ribosomal frameshifting (PRF) results in the −1 reading frame. In most cases of −1 PRF, two mRNA features are necessary to induce efficient frameshifting (25). First, a slippery sequence which allows codon–anticodon base-pairing between the mRNA and the bound tRNAs in the 0 frame and the −1 frame. Second, a frameshift stimulating sequence (FSS) located downstream of the slippery sequence slows down the progression of the ribosome. FSS elements are stable mRNA secondary structure elements ranging from simple stem loops to more complex pseudoknots.

Several MD simulation studies of isolated frameshift-stimulating pseudoknots have been carried out (16, 46, 74, 75, 85, 86, 141, 150, 171, 172, 208, 221). Gupta et al. (74) and Kim et al. (104) simulated the wild-type pseudoknot of the *Beet Western Yellow Virus* as well as four mutated variants that were previously found to either increase or decrease frameshift efficiencies. In the simulations, the mutations resulted in local conformational changes, while the overall fold of the pseudoknot was not affected within the simulation time of 200 ns. The results suggested that either the simulation time is shorter than unfolding or refolding timescales or the local changes interfered with the pseudoknot–ribosome interaction, resulting in altered frameshift efficiencies. Zhong et al. (221) combined thermal melting experiments, optical tweezers experiments, and MD simulations to study the thermal and mechanical stability of the gap-pro mRNA pseudoknot of the *Simian Retrovirus type 1*. While the thermal stability of the different sequence variants of the pseudoknot did not show a correlation with the frameshift efficiency, they found a strong correlation between the frameshift efficiency and the unfolding rate of the pseudoknot. Interestingly, the correlation was highest for unfolding rates at pulling forces in the range of 13–35 pN, which is close to the approximately 13 pN force that the ribosome can generate during tRNA–mRNA translocation (122). These results suggest that the time during which the ribosome is stalled and can cross the free-energy barrier to the −1 frame is determined by the lifetime of the pseudoknot. In turn, the lifetime of the pseudoknot is determined by the unfolding rate under the force generated by the ribosome.

Before any structure of the SARS-CoV-1 pseudoknot was resolved, Park et al. (152) predicted a structural model and carried out short MD simulations. The resulting structure was used as a target for virtual screening of approximately 80,000 compounds. The active site for the virtual screening was chosen to be centered around nucleotides of the pseudoknot previously shown to be important for frameshifting. A set of 58 highly ranked compounds was tested in vitro; one compound was identified to reduce the frameshift efficiency by 80%. This result highlights the FSS elements as potential targets for antiviral drugs.

Omar et al. (150) used six different structure prediction platforms to model the structure of the SARS-CoV-2 pseudoknot. The modeled structures, which varied in their fold topologies, were

then used as starting structures for microsecond-long MD simulations. The stability of the secondary structure and tertiary contacts during the simulations was used as a criterion to estimate which topologies are more likely. In particular, two distinct fold topologies were found to be stable throughout the simulations, one with the 5′ end threaded through the junction between stem loops S1 and S3 and the other without any threading. These results suggest that both topologies might be stable on the timescales relevant for frameshifting, presumably with different effects on the frameshift efficiencies.

Together, studies using MD simulations (150, 172), X-ray crystallography (93), and cryo-EM (219) suggest that the isolated SARS-CoV-2 pseudoknot can adopt a large range of conformations, which can be quite different from its conformation in the presence of the ribosome (19). The studies suggest that the energetics and dynamics of the isolated FSSs without the context of the ribosome do not suffice to fully explain how different variants of FSS involved in different frameshift events result in different frameshift efficiencies. Chang et al. (39) combined short MD simulations of the ribosome in complex with the human telomerase RNA pseudoknot, normal mode analysis, and linear response theory to estimate the motion of the ribosome under the force resulting from unwinding intermediates of the pseudoknot. Based on their results, they proposed that the tension built up during the structural unfolding of the pseudoknot induced a 30S subunit rolling and distorted tRNAs, which then resulted in tRNA slippage on the slippery sequence.

High-resolution structures of FSS in the context of the ribosome are available for dnaX (220), HIV (12), and SARS-CoV-2 (19). Future aaMD simulations begun from these available structures with and without mutations known to affect the frameshift efficiency will allow researchers to study how the ribosome–FSS interactions contribute to the frameshift.

Substantial ribosomal frameshifting can also be induced in the absence of FSS downstream of the slippery sequence (42). Harrington et al. (77) suggested that −1 frameshifting can be induced by the membrane integration of the transmembrane domain upstream of the slippery sequence. Using a combination of biochemical and cellular techniques, they suggested that the hydrophobicity of the transmembrane and the sequence length between domain and slippery sequence both affect the frameshift efficiency. Based on cgMD simulations, they estimated the forces that act on the NC and are generated by the membrane integration of different transmembrane domain variants. The forces showed a high correlation with the frameshift efficiency. Carmody et al. (34) used deep mutational scanning to measure −1 PRF efficiencies of 4,530 mutations of the slippery site, as well as mutations upstream and downstream of the slippery site. Based on cgMD and aaMD simulations of growing NCs within the outer part of the exit tunnel and the translocon, they suggested that the effects of upstream mutations are due to the forces generated by translocon-mediated cotranslational folding of the NC.

To date, only a few MD simulation studies have focused on the role that the mRNA–tRNA interactions play during frameshifting. In *Escherichia coli*, $tRNA^{Ser3}$, with a GCU anticodon, can induce −1 frameshifting at an alanine codon (GCA) (26). To explain this frameshifting event, a doublet model was proposed in which the codon nucleotides G1 and C2 pair with anticodon nucleotides C35 and U34, respectively. The next tRNA would then decode the mRNA in the −1 frame. However, the doublet model could not explain why a mutation of anticodon nucleotide U36 to C, which, based on the model, does not participate in the mechanism, prevents the frameshift. Based on MD simulations of different codon–anticodon pairs in the ribosomal A site, Caulfield et al. (36) proposed that, when $tRNA^{Ser3}$ is bound, the G1 nucleotide forms hydrogen bonds with both U36 and U35 and that, therefore, the identity of U36 is crucial for this type of frameshifting.

It has been shown recently that the efficiency of shifting the reading frame of the ribosome during −1 PRF in the presence of the dnaX pseudoknot depends on—and can in fact be predicted

from—the free energies of the codon–anticodon base pairs present in the different reading frames (22). Using a Bayes approach, it was shown that the base-pair free-energy differences can be obtained from measured frameshifting efficiencies. These free-energy differences would provide an independent control for MD-based free-energy calculations of the base-pair interactions, with implications not only for frameshifting, but also for the kinetics of decoding.

4. CONCLUSIONS

Molecular simulations have the potential to integrate the results from various experimental techniques into a detailed and predictive model of a macromolecular biological process. To fully realize this potential, the simulation model has to be a sufficiently accurate in silico representation of the experiment. We see room for improvement along several lines.

One of the classic challenges is, of course, to match the time- and length scales of the MD simulations and the experiments. Given the ongoing current advances in algorithms and hardware, atomistic MD simulations of large biomolecular complexes such as the ribosome will reach millisecond timescales in the near future. Similarly, current and expected future improvements in the time resolution of experiments will help to further close the gap between simulation and experiment.

However, a close match of timescales is not always required. Consider processes that reach equilibrium rapidly, e.g., the conformational dynamics of a growing nascent peptide in the ribosomal exit tunnel (84). In this case, an equilibrium ensemble of conformations is likely to be reached on timescales much shorter than the tenths of a second rates by which elongation proceeds, such that correspondingly shorter simulations will suffice. Of course, the timescales of conformational changes are hard to predict before carrying out the actual simulations. As another example, for the large-scale conformational changes in intersubunit rotation and L1-stalk dynamics, substantial motion was already observed on the 100-ns timescale (20, 21, 209). However, the relatively small and localized conformational changes of NC rearrangement after removal of an antibiotic do not equilibrate within several microseconds, and therefore many replicates in the simulation protocol were required to obtain sufficient statistics (10, 13).

Other options to mimic the experiment include fluorescence spectroscopy and EPR experiments. In these cases, explicit inclusion of the dye or spin label (76, 80, 82) is not yet state of the art. This explicit inclusion not only provides for a more realistic model of the experimental condition, but also allows one to drop assumptions, e.g., the orientational and distance distribution of the mutual orientation of dyes in FRET experiments, as well as their dynamics. Ideally, this approach allows one to drop the often problematic $\kappa^2 = 2/3$-assumption, replacing it by the simulation result. Such direct modeling approaches therefore allow for a more direct comparison between the simulations and experiments.

These examples shine a light on a general principle, the power of which is being increasingly recognized and exploited: Rather than comparing interpreted quantities from experiment to simulation (e.g., FRET or NMR distances), which always requires additional assumptions that may or may not be fulfilled and are often difficult to assess, it is better to compare the measured raw data (FRET efficiencies, NMR NOEs, or relaxation spectra) with those calculated from simulations. Whereas mismatch between interpreted quantities may have many causes in either the experiment or the simulation, mismatch of raw data must be blamed on the simulation and is, thus, easier to resolve. If or when agreement is achieved, the simulation can be used to provide a structural causal interpretation of the experiment.

Such a raw data approach requires particular attention to all the details of the experiment that may affect the direct comparison. For example, the conformational ensemble of biomolecules captured by cryo-EM depends not only on the cryogenic temperature, but also on the temperature

before cooling, as well as on the cooling rate (23, 40, 41, 57, 139, 180). Thus, the conformational heterogeneity and the population of states observed in cryo-EM experiments do not necessarily reflect the room-temperature ensemble probed by simulations. In this case, use of proper kinetic models to connect the two structure distributions (23) promises to reveal deeper insights into the free-energy landscape that governs the functional dynamics of the ribosome.

Both advancing simulation techniques toward a 1:1 description of experiments and advancing experiments to facilitate this process will be key to develop an understanding of the function of large-scale biomolecules from fundamental physics.

DISCLOSURE STATEMENT

The authors are not aware of any affiliations, memberships, funding, or financial holdings that might be perceived as affecting the objectivity of this review.

ACKNOWLEDGMENTS

This work was funded by the Deutsche Forschungsgemeinschaft (DFG, German Research Foundation) under Germany's Excellence Strategy, grant EXC 2067/1-390729940 (to L.V.B. and H.G.). M.H.K. acknowledges the support of the Czech Science Foundation (project 19-06479Y). We thank Carsten Kutzner, Edward P. O'Brien, Paul Whitford, and Karissa Sanbonmatsu for discussions and critical reading of the manuscript.

LITERATURE CITED

1. Abeysirigunawardena SC, Kim H, Lai J, Ragunathan K, Rappé MC, et al. 2017. Evolution of protein-coupled RNA dynamics during hierarchical assembly of ribosomal complexes. *Nat. Commun.* 8:492
2. Aduri R, Psciuk BT, Saro P, Taniga H, Schlegel HB, SantaLucia J. 2007. AMBER force field parameters for the naturally occurring modified nucleosides in RNA. *J. Chem. Theory Comput.* 3(4):1464–75
3. Agashe VR, Guha S, Chang HC, Genevaux P, Hayer-Hartl M, et al. 2004. Function of trigger factor and DnaK in multidomain protein folding: increase in yield at the expense of folding speed. *Cell* 117(2):199–209
4. Agris PF, Vendeix FA, Graham WD. 2007. tRNA's wobble decoding of the genome: 40 years of modification. *J. Mol. Biol.* 366(1):1–13
5. Alderson TR, Kay LE. 2021. NMR spectroscopy captures the essential role of dynamics in regulating biomolecular function. *Cell* 184(3):577–95
6. Åqvist J, Kamerlin SCL. 2015. The conformation of a catalytic loop is central to GTPase activity on the ribosome. *Biochemistry* 54(2):546–56
7. Åqvist J, Kamerlin SCL. 2015. Exceptionally large entropy contributions enable the high rates of GTP hydrolysis on the ribosome. *Sci. Rep.* 5:15817
8. Åqvist J, Kamerlin SCL. 2016. Conserved motifs in different classes of GTPases dictate their specific modes of catalysis. *ACS Catal.* 6(3):1737–43
9. Åqvist J, Lind C, Sund J, Wallin G. 2012. Bridging the gap between ribosome structure and biochemistry by mechanistic computations. *Curr. Opin. Struct. Biol.* 22(6):815–23
10. Arenz S, Bock LV, Graf M, Innis CA, Beckmann R, et al. 2016. A combined cryo-EM and molecular dynamics approach reveals the mechanism of ErmBL-mediated translation arrest. *Nat. Commun.* 7:12026
11. B RP, Plotnikov NV, Lameira J, Warshel A. 2013. Quantitative exploration of the molecular origin of the activation of GTPase. *PNAS* 110(51):20509–14
12. Bao C, Loerch S, Ling C, Korostelev AA, Grigorieff N, Ermolenko DN. 2020. mRNA stem-loops can pause the ribosome by hindering A-site tRNA binding. *eLife* 9:e55799
13. Beckert B, Leroy EC, Sothiselvam S, Bock LV, Svetlov MS, et al. 2021. Structural and mechanistic basis for translation inhibition by macrolide and ketolide antibiotics. *Nat. Commun.* 12:4466

14. Belardinelli R, Sharma H, Caliskan N, Cunha CE, Peske F, et al. 2016. Choreography of molecular movements during ribosome progression along mRNA. *Nat. Struct. Mol. Biol.* 23(4):342–48
15. Belardinelli R, Sharma H, Peske F, Wintermeyer W, Rodnina MV. 2016. Translocation as continuous movement through the ribosome. *RNA Biol.* 13(12):1197–203
16. Belew AT, Meskauskas A, Musalgaonkar S, Advani VM, Sulima SO, et al. 2014. Ribosomal frameshifting in the CCR5 mRNA is regulated by miRNAs and the NMD pathway. *Nature* 512(7514):265–69
17. Bernardi RC, Melo MC, Schulten K. 2015. Enhanced sampling techniques in molecular dynamics simulations of biological systems. *Biochim. Biophys. Acta Gen. Subj.* 1850(5):872–77
18. Best RB, Zhu X, Shim J, Lopes PE, Mittal J, et al. 2012. Optimization of the additive CHARMM all-atom protein force field targeting improved sampling of the backbone ϕ, ψ and side-chain $\chi 1$ and $\chi 2$ dihedral angles. *J. Chem. Theory Comput.* 8(9):3257–73
19. Bhatt PR, Scaiola A, Loughran G, Leibundgut M, Kratzel A, et al. 2021. Structural basis of ribosomal frameshifting during translation of the SARS-CoV-2 RNA genome. *Science* 372(6548):1306–13
20. Bock LV, Blau C, Schröder GF, Davydov II, Fischer N, et al. 2013. Energy barriers and driving forces in tRNA translocation through the ribosome. *Nat. Struct. Mol. Biol.* 20(12):1390–96
21. Bock LV, Blau C, Vaiana AC, Grubmüller H. 2015. Dynamic contact network between ribosomal subunits enables rapid large-scale rotation during spontaneous translocation. *Nucleic Acids Res.* 43(14):6747–60
22. Bock LV, Caliskan N, Korniy N, Peske F, Rodnina MV, Grubmüller H. 2019. Thermodynamic control of −1 programmed ribosomal frameshifting. *Nat. Commun.* 10:4598
23. Bock LV, Grubmüller H. 2022. Effects of cryo-EM cooling on structural ensembles. *Nat. Commun.* 13:1709
24. Bock LV, Kolár MH, Grubmüller H. 2018. Molecular simulations of the ribosome and associated translation factors. *Curr. Opin. Struct. Biol.* 49:27–35
25. Brierley I. 1995. Ribosomal frameshifting on viral RNAs. *J. Gen. Virol.* 76(8):1885–92
26. Bruce AG, Atkins JF, Gesteland RF. 1986. tRNA anticodon replacement experiments show that ribosomal frameshifting can be caused by doublet decoding. *PNAS* 83(14):5062–66
27. Bui PT, Hoang TX. 2016. Folding and escape of nascent proteins at ribosomal exit tunnel. *J. Chem. Phys.* 144(9):095102
28. Bui PT, Hoang TX. 2018. Protein escape at the ribosomal exit tunnel: effects of native interactions, tunnel length, and macromolecular crowding. *J. Chem. Phys.* 149(4):045102
29. Bui PT, Hoang TX. 2020. Protein escape at the ribosomal exit tunnel: effect of the tunnel shape. *J. Chem. Phys.* 153(4):045105
30. Bustamante C, Alexander L, Maciuba K, Kaiser CM. 2020. Single-molecule studies of protein folding with optical tweezers. *Annu. Rev. Biochem.* 89:443–70
31. Cabrita LD, Cassaignau AM, Launay HM, Waudby CA, Wlodarski T, et al. 2016. A structural ensemble of a ribosome–nascent chain complex during cotranslational protein folding. *Nat. Struct. Mol. Biol.* 23(4):278–85
32. Cabrita LD, Hsu STD, Launay H, Dobson CM, Christodoulou J. 2009. Probing ribosome-nascent chain complexes produced in vivo by NMR spectroscopy. *PNAS* 106(52):22239–44
33. Camilloni C, Cavalli A, Vendruscolo M. 2013. Replica-averaged metadynamics. *J. Chem. Theory Comput.* 9(12):5610–17
34. Carmody PJ, Zimmer MH, Kuntz CP, Harrington HR, Duckworth KE, et al. 2021. Coordination of −1 programmed ribosomal frameshifting by transcript and nascent chain features revealed by deep mutational scanning. *Nucleic Acids Res.* 49(22):12943–54
35. Cassaignau AM, Włodarski T, Chan SH, Woodburn LF, Bukvin IV, et al. 2021. Interactions between nascent proteins and the ribosome surface inhibit co-translational folding. *Nat. Chem.* 13(12):1214–20
36. Caulfield T, Coban M, Tek A, Flores SC. 2019. Molecular dynamics simulations suggest a non-doublet decoding model of −1 frameshifting by $tRNA^{Ser3}$. *Biomolecules* 9(11):745
37. Chan SH, Waudby CA, Christodoulou J. 2022. NMR snapshots of nascent chains emerging from the ribosome during biosynthesis. ChemRxiv. **https://doi.org/10.26434/chemrxiv-2022-0lmsp**
38. Chan SH, Włodarski T, Streit JO, Cassaignau AM, Woodburn LF, et al. 2022. The ribosome stabilizes partially folded intermediates of a nascent multi-domain protein. *Nat. Chem.* 14(10):1165–73

39. Chang KC, Salawu EO, Chang YY, Wen JD, Yang LW. 2019. Resolution-exchanged structural modeling and simulations jointly unravel that subunit rolling underlies the mechanism of programmed ribosomal frameshifting. *Bioinformatics* 35(6):945–52
40. Chen CY, Chang YC, Lin BL, Huang CH, Tsai MD. 2019. Temperature-resolved cryo-EM uncovers structural bases of temperature-dependent enzyme functions. *J. Am. Chem. Soc.* 141(51):19983–87
41. Chu X, Su X, Liu M, Li L, Li T, et al. 2022. Annealing synchronizes the 70S ribosome into a minimum-energy conformation. *PNAS* 119(8):e2111231119
42. Chung BY, Firth AE, Atkins JF. 2010. Frameshifting in alphaviruses: a diversity of 3′ stimulatory structures. *J. Mol. Biol.* 397(2):448–56
43. Clark PL. 2004. Protein folding in the cell: reshaping the folding funnel. *Trends Biochem. Sci.* 29(10):527–34
44. Cohen AJ, Mori-Sánchez P, Yang W. 2012. Challenges for density functional theory. *Chem. Rev.* 112(1):289–320
45. Cornish PV, Ermolenko DN, Noller HF, Ha T. 2008. Spontaneous intersubunit rotation in single ribosomes. *Mol. Cell* 30(5):578–88
46. Csaszar K, Špačková N, Štefl R, Šponer J, Leontis NB. 2001. Molecular dynamics of the frame-shifting pseudoknot from beet western yellows virus: the role of non-Watson-Crick base-pairing, ordered hydration, cation binding and base mutations on stability and unfolding. *J. Mol. Biol.* 313(5):1073–91
47. Cunha CE, Belardinelli R, Peske F, Holtkamp W, Wintermeyer W, Rodnina MV. 2013. Dual use of GTP hydrolysis by elongation factor G on the ribosome. *Translation* 1(1):e24315
48. Daviter T, Wieden HJ, Rodnina MV. 2003. Essential role of histidine 84 in elongation factor Tu for the chemical step of GTP hydrolysis on the ribosome. *J. Mol. Biol.* 332(3):689–99
49. de Jong DH, Baoukina S, Ingólfsson HI, Marrink SJ. 2016. Martini straight: boosting performance using a shorter cutoff and GPUs. *Comput. Phys. Commun.* 199:1–7
50. Deckert A, Cassaignau AME, Wang X, Włodarski T, Chan SHS, et al. 2021. Common sequence motifs of nascent chains engage the ribosome surface and trigger factor. *PNAS* 118(52):e2103015118
51. Deckert A, Waudby CA, Włodarski T, Wentink AS, Wang X, et al. 2016. Structural characterization of the interaction of α-synuclein nascent chains with the ribosomal surface and trigger factor. *PNAS* 113(18):5012–17
52. Deeng J, Chan KY, van der Sluis EO, Berninghausen O, Han W, et al. 2016. Dynamic behavior of trigger factor on the ribosome. *J. Mol. Biol.* 428(18):3588–602
53. Di Palma F, Decherchi S, Pardo-Avila F, Succi S, Levitt M, et al. 2021. Probing interplays between human XBP1u translational arrest peptide and 80S ribosome. *J. Chem. Theory Comput.* 18(3):1905–14
54. Doster W, Cusack S, Petry W. 1989. Dynamical transition of myoglobin revealed by inelastic neutron scattering. *Nature* 337(6209):754–56
55. Dror RO, Dirks RM, Grossman J, Xu H, Shaw DE. 2012. Biomolecular simulation: a computational microscope for molecular biology. *Annu. Rev. Biophys.* 41:429–52
56. Englander MT, Avins JL, Fleisher RC, Liu B, Effraim PR, et al. 2015. The ribosome can discriminate the chirality of amino acids within its peptidyl-transferase center. *PNAS* 112(19):6038–43
57. Fischer N, Konevega AL, Wintermeyer W, Rodnina MV, Stark H. 2010. Ribosome dynamics and tRNA movement by time-resolved electron cryomicroscopy. *Nature* 466(7304):329–33
58. Fischer N, Neumann P, Bock LV, Maracci C, Wang Z, et al. 2016. The pathway to GTPase activation of elongation factor SelB on the ribosome. *Nature* 540(7631):80–85
59. Fischer N, Neumann P, Konevega AL, Bock LV, Ficner R, et al. 2015. Structure of the *E. coli* ribosome–EF-Tu complex at <3 Å resolution by Cs-corrected cryo-EM. *Nature* 520(7548):567–70
60. Fogolari F, Brigo A, Molinari H. 2002. The Poisson-Boltzmann equation for biomolecular electrostatics: a tool for structural biology. *J. Mol. Recognit.* 15(6):377–92
61. Förster T. 1948. Zwischenmolekulare Energiewanderung und Fluoreszenz. *Ann. Phys.* 437(1–2):55–75
62. Frauenfelder H, Parak F, Young RD. 1988. Conformational substates in proteins. *Annu. Rev. Biophys. Biophys. Chem.* 17:451–79
63. Freitas FC, Fuchs G, de Oliveira RJ, Whitford PC. 2021. The dynamics of subunit rotation in a eukaryotic ribosome. *Biophysica* 1(2):204–21

64. Frenkel D, Smit B. 2001. *Understanding Molecular Simulation: From Algorithms to Applications*, Vol. 1. Amsterdam: Elsevier
65. Fries SJ, Braun TS, Globisch C, Peter C, Drescher M, Deuerling E. 2021. Deciphering molecular details of the RAC–ribosome interaction by EPR spectroscopy. *Sci. Rep.* 11:8681
66. Gao YG, Selmer M, Dunham CM, Weixlbaumer A, Kelley AC, Ramakrishnan V. 2009. The structure of the ribosome with elongation factor G trapped in the posttranslocational state. *Science* 326(5953):694–99
67. Gaus M, Cui Q, Elstner M. 2014. Density functional tight binding: application to organic and biological molecules. *Wiley Interdiscip. Rev. Comput. Mol. Sci.* 4(1):49–61
68. Ge X, Mandava CS, Lind C, Åqvist J, Sanyal S. 2018. Complementary charge-based interaction between the ribosomal-stalk protein L7/12 and IF2 is the key to rapid subunit association. *PNAS* 115(18):4649–54
69. Giraldo-Barreto J, Ortiz S, Thiede EH, Palacio-Rodriguez K, Carpenter B, et al. 2021. A Bayesian approach to extracting free-energy profiles from cryo-electron microscopy experiments. *Sci. Rep.* 11:13657
70. Go N. 1983. Theoretical studies of protein folding. *Annu. Rev. Biophys. Bioeng.* 12:183–210
71. Gogonea V, Suárez D, van der Vaart A, Merz KM Jr. 2001. New developments in applying quantum mechanics to proteins. *Curr. Opin. Struct. Biol.* 11(2):217–23
72. Goldman DH, Kaiser CM, Milin A, Righini M, Tinoco I, Bustamante C. 2015. Mechanical force releases nascent chain-mediated ribosome arrest in vitro and in vivo. *Science* 348(6233):457–60
73. Gopich IV, Szabo A. 2012. Theory of the energy transfer efficiency and fluorescence lifetime distribution in single-molecule FRET. *PNAS* 109(20):7747–52
74. Gupta A, Bansal M. 2014. Local structural and environmental factors define the efficiency of an RNA pseudoknot involved in programmed ribosomal frameshift process. *J. Phys. Chem. B* 118(41):11905–20
75. Gupta A, Bansal M. 2016. The role of sequence in altering the unfolding pathway of an RNA pseudoknot: a steered molecular dynamics study. *Phys. Chem. Chem. Phys.* 18(41):28767–80
76. Halbmair K, Seikowski J, Tkach I, Höbartner C, Sezer D, Bennati M. 2016. High-resolution measurement of long-range distances in RNA: pulse EPR spectroscopy with TEMPO-labeled nucleotides. *Chem. Sci.* 7(5):3172–80
77. Harrington HR, Zimmer MH, Chamness LM, Nash V, Penn WD, et al. 2020. Cotranslational folding stimulates programmed ribosomal frameshifting in the alphavirus structural polyprotein. *J. Biol. Chem.* 295(20):6798–808
78. Hartono YD, Ito M, Villa A, Nilsson L. 2018. Computational study of uracil tautomeric forms in the ribosome: the case of uracil and 5-oxyacetic acid uracil in the first anticodon position of tRNA. *J. Phys. Chem. B* 122(3):1152–60
79. Hassan A, Byju S, Whitford PC. 2021. The energetics of subunit rotation in the ribosome. *Biophys. Rev.* 13(6):1029–37
80. Heinz M, Erlenbach N, Stelzl LS, Thierolf G, Kamble NR, et al. 2020. High-resolution EPR distance measurements on RNA and DNA with the non-covalent G′ spin label. *Nucleic Acids Res.* 48(2):924–33
81. Hensen U, Meyer T, Haas J, Rex R, Vriend G, Grubmüller H. 2012. Exploring protein dynamics space: the dynasome as the missing link between protein structure and function. *PLOS ONE* 7(5):e33931
82. Hoefling M, Lima N, Haenni D, Seidel CA, Schuler B, Grubmüller H. 2011. Structural heterogeneity and quantitative FRET efficiency distributions of polyprolines through a hybrid atomistic simulation and Monte Carlo approach. *PLOS ONE* 6(5):e19791
83. Holtkamp W, Cunha CE, Peske F, Konevega AL, Wintermeyer W, Rodnina MV. 2014. GTP hydrolysis by EF-G synchronizes tRNA movement on small and large ribosomal subunits. *EMBO J.* 33(9):1073–85
84. Holtkamp W, Kokic G, Jager M, Mittelstaet J, Komar AA, Rodnina MV. 2015. Cotranslational protein folding on the ribosome monitored in real time. *Science* 350(6264):1104–7
85. Hori N, Denesyuk NA, Thirumalai D. 2016. Salt effects on the thermodynamics of a frameshifting RNA pseudoknot under tension. *J. Mol. Biol.* 428(14):2847–59
86. Hsu CF, Chang KC, Chen YL, Hsieh PS, Lee AI, et al. 2021. Formation of frameshift-stimulating RNA pseudoknots is facilitated by remodeling of their folding intermediates. *Nucleic Acids Res.* 49(12):6941–57
87. Huter P, Arenz S, Bock LV, Graf M, Frister JO, et al. 2017. Structural basis for polyproline-mediated ribosome stalling and rescue by the translation elongation factor EF-P. *Mol. Cell* 68(3):515–27

88. Igaev M, Kutzner C, Bock LV, Vaiana AC, Grubmüller H. 2019. Automated cryo-EM structure refinement using correlation-driven molecular dynamics. *eLife* 8:e43542
89. Imai H, Uchiumi T, Kodera N. 2020. Direct visualization of translational GTPase factor pool formed around the archaeal ribosomal P-stalk by high-speed AFM. *PNAS* 117(51):32386–94
90. Invernizzi M, Piaggi PM, Parrinello M. 2020. Unified approach to enhanced sampling. *Phys. Rev. X* 10(4):041034
91. Jiang Y, O'Brien EP. 2021. Mechanical forces have a range of effects on the rate of ribosome catalyzed peptidyl transfer depending on direction. *J. Phys. Chem. B* 125(26):7128–36
92. Jo S, Kim T, Iyer VG, Im W. 2008. CHARMM-GUI: a web-based graphical user interface for CHARMM. *J. Comput. Chem.* 29(11):1859–65
93. Jones CP, Ferré-D'amaré AR. 2022. Crystal structure of the severe acute respiratory syndrome coronavirus 2 (SARS-CoV-2) frameshifting pseudoknot. *RNA* 28(2):239–49
94. Jones RO. 2015. Density functional theory: its origins, rise to prominence, and future. *Rev. Mod. Phys.* 87(3):897
95. Juette MF, Terry DS, Wasserman MR, Zhou Z, Altman RB, et al. 2014. The bright future of single-molecule fluorescence imaging. *Curr. Opin. Chem. Biol.* 20(1):103–11
96. Kalinin S, Peulen T, Sindbert S, Rothwell PJ, Berger S, et al. 2012. A toolkit and benchmark study for FRET-restrained high-precision structural modeling. *Nat. Methods* 9(12):1218–25
97. Karplus M, McCammon JA. 2002. Molecular dynamics simulations of biomolecules. *Nat. Struct. Biol.* 9(9):646–52
98. Karplus M, Petsko GA. 1990. Molecular dynamics simulations in biology. *Nature* 347(6294):631–39
99. Kästner J, Sherwood P. 2010. The ribosome catalyzes peptide bond formation by providing high ionic strength. *Mol. Phys.* 108(3–4):293–306
100. Kazantsev A, Ignatova Z. 2021. Constraints on error rate revealed by computational study of G • U tautomerization in translation. *Nucleic Acids Res.* 1(1256879):13–14
101. Kazemi M, Himo F, Åqvist J. 2016. Peptide release on the ribosome involves substrate-assisted base catalysis. *ACS Catal.* 6(12):8432–39
102. Kim DN, Moriarty NW, Kirmizialtin S, Afonine PV, Poon B, et al. 2019. Cryo_fit: democratization of flexible fitting for cryo-EM. *J. Struct. Biol.* 208(1):1–6
103. Kim H, Abeysirigunawarden SC, Chen K, Mayerle M, Ragunathan K, et al. 2014. Protein-guided RNA dynamics during early ribosome assembly. *Nature* 506(7488):334–38
104. Kim YG, Su L, Maas S, O'Neill A, Rich A. 1999. Specific mutations in a viral RNA pseudoknot drastically change ribosomal frameshifting efficiency. *PNAS* 96(25):14234–39
105. Koehl P. 2006. Electrostatics calculations: latest methodological advances. *Curr. Opin. Struct. Biol.* 16(2):142–51
106. Kolář MH, Nagy G, Kunkel J, Vaiana SM, Bock LV, Grubmüller H. 2022. Folding of VemP into translation-arresting secondary structure is driven by the ribosome exit tunnel. *Nucleic Acids Res.* 50(4):2258–69
107. Korostelev AA. 2022. The structural dynamics of translation. *Annu. Rev. Biochem.* 91:245–67
108. Kuhlenkoetter S, Wintermeyer W, Rodnina MV. 2011. Different substrate-dependent transition states in the active site of the ribosome. *Nature* 476(7360):351–54
109. Kurland C. 1992. Translational accuracy and the fitness of bacteria. *Annu. Rev. Genet.* 26:29–50
110. Kutzner C, Páll S, Fechner M, Esztermann A, de Groot BL, Grubmüller H. 2019. More bang for your buck: improved use of GPU nodes for GROMACS 2018. *J. Comput. Chem.* 40(27):2418–31
111. Leininger SE, Rodriguez J, Vu QV, Jiang Y, Li MS, et al. 2021. Ribosome elongation kinetics of consecutively charged residues are coupled to electrostatic force. *Biochemistry* 60(43):3223–35
112. Levi M, Nguyen K, Dukaye L, Whitford PC. 2017. Quantifying the relationship between single-molecule probes and subunit rotation in the ribosome. *Biophys. J.* 113(12):2777–86
113. Levi M, Noel JK, Whitford PC. 2019. Studying ribosome dynamics with simplified models. *Methods* 162:128–40
114. Levi M, Walak K, Wang A, Mohanty U, Whitford PC. 2020. A steric gate controls P/E hybrid-state formation of tRNA on the ribosome. *Nat. Commun.* 11:5706

115. Levi M, Whitford PC. 2019. Dissecting the energetics of subunit rotation in the ribosome. *J. Phys. Chem. B* 123(13):2812–23
116. Levine IN, Busch DH, Shull H. 2009. *Quantum Chemistry*, Vol. 6. Hoboken, NJ: Prentice Hall
117. Lin J, Zhou D, Steitz TA, Polikanov YS, Gagnon MG. 2018. Ribosome-targeting antibiotics: modes of action, mechanisms of resistance, and implications for drug design. *Annu. Rev. Biochem.* 87:451–78
118. Lind C, Åqvist J. 2016. Principles of start codon recognition in eukaryotic translation initiation. *Nucleic Acids Res.* 44(17):8425–32
119. Lind C, Oliveira A, Åqvist J. 2017. Origin of the omnipotence of eukaryotic release factor 1. *Nat. Commun.* 8:1425
120. Lindorff-Larsen K, Best RB, DePristo MA, Dobson CM, Vendruscolo M. 2005. Simultaneous determination of protein structure and dynamics. *Nature* 433(7022):128–32
121. Liu K, Chen X, Kaiser CM. 2019. Energetic dependencies dictate folding mechanism in a complex protein. *PNAS* 116(51):25641–48
122. Liu T, Kaplan A, Alexander L, Yan S, Wen JD, et al. 2014. Direct measurement of the mechanical work during translocation by the ribosome. *eLife* 3:e03406
123. Liutkute M, Samatova E, Rodnina MV. 2020. Cotranslational folding of proteins on the ribosome. *Biomolecules* 10(1):97
124. Lu J, Deutsch C. 2008. Electrostatics in the ribosomal tunnel modulate chain elongation rates. *J. Mol. Biol.* 384(1):73–86
125. Maier JA, Martinez C, Kasavajhala K, Wickstrom L, Hauser KE, Simmerling C. 2015. ff14SB: improving the accuracy of protein side chain and backbone parameters from ff99SB. *J. Chem. Theory Comput.* 11(8):3696–713
126. Makarov GI, Makarova TM, Sumbatyan NV, Bogdanov AA. 2016. Investigation of ribosomes using molecular dynamics simulation methods. *Biochemistry* 81(13):1579–88
127. Malygin AA, Graifer DM, Meschaninova MI, Venyaminova AG, Krumkacheva OA, et al. 2015. Doubly spin-labeled RNA as an EPR reporter for studying multicomponent supramolecular assemblies. *Biophys. J.* 109(12):2637–43
128. Malygin AA, Graifer DM, Meschaninova MI, Venyaminova AG, Timofeev IO, et al. 2018. Structural rearrangements in mRNA upon its binding to human 80S ribosomes revealed by EPR spectroscopy. *Nucleic Acids Res.* 46(2):897–904
129. Malygin AA, Krumkacheva OA, Graifer DM, Timofeev IO, Ochkasova AS, et al. 2019. Exploring the interactions of short RNAs with the human 40S ribosomal subunit near the mRNA entry site by EPR spectroscopy. *Nucleic Acids Res.* 47(22):11850–60
130. Maracci C, Peske F, Dannies E, Pohl C, Rodnina MV. 2014. Ribosome-induced tuning of GTP hydrolysis by a translational GTPase. *PNAS* 111(40):14418–23
131. Marrink SJ, De Vries AH, Mark AE. 2004. Coarse grained model for semiquantitative lipid simulations. *J. Phys. Chem. B* 108(2):750–60
132. Marrink SJ, Risselada HJ, Yefimov S, Tieleman DP, De Vries AH. 2007. The MARTINI force field: coarse grained model for biomolecular simulations. *J. Phys. Chem. B* 111(27):7812–24
133. Marrink SJ, Tieleman DP. 2013. Perspective on the Martini model. *Chem. Soc. Rev.* 42(16):6801–22
134. Marshall RA, Dorywalska M, Puglisi JD. 2008. Irreversible chemical steps control intersubunit dynamics during translation. *PNAS* 105(40):15364–69
135. McGrath H, Černeková M, Kolář MH. 2022. Binding of the peptide deformylase on the ribosome surface modulates the exit tunnel interior. *Biophys. J.* 121(23):4443–51
136. Mondal D, Warshel A. 2018. EF-Tu and EF-G are activated by allosteric effects. *PNAS* 115(13):3386–91
137. Munro JB, Altman RB, O'Connor N, Blanchard SC. 2007. Identification of two distinct hybrid state intermediates on the ribosome. *Mol. Cell* 25(4):505–17
138. Munro JB, Vaiana A, Sanbonmatsu KY, Blanchard SC. 2008. A new view of protein synthesis: mapping the free energy landscape of the ribosome using single-molecule FRET. *Biopolymers* 89(7):565–77
139. Nadezhdin KD, Neuberger A, Trofimov YA, Krylov NA, Sinica V, et al. 2021. Structural mechanism of heat-induced opening of a temperature-sensitive TRP channel. *Nat. Struct. Mol. Biol.* 28(7):564–72
140. Nguyen K, Whitford PC. 2016. Steric interactions lead to collective tilting motion in the ribosome during mRNA–tRNA translocation. *Nat. Commun.* 7:10586

141. Nguyen KKQ, Gomez YK, Bakhom M, Radcliffe A, La P, et al. 2017. Ensemble simulations: folding, unfolding and misfolding of a high-efficiency frameshifting RNA pseudoknot. *Nucleic Acids Res.* 45(8):4893–904
142. Niesen MJM, Müller-Lucks A, Hedman R, von Heijne G, Miller TF. 2018. Forces on nascent polypeptides during membrane insertion and translocation via the Sec translocon. *Biophys. J.* 115(10):1885–94
143. Niesen MJM, Wang CY, Van Lehn RC, Miller TF. 2017. Structurally detailed coarse-grained model for Sec-facilitated co-translational protein translocation and membrane integration. *PLOS Comput. Biol.* 13(3):e1005427
144. Nissley DA, Jiang Y, Trovato F, Sitarik I, Narayan KB, et al. 2022. Universal protein misfolding intermediates can bypass the proteostasis network and remain soluble and less functional. *Nat. Commun.* 13:3081
145. Nissley DA, O'Brien EP. 2018. Structural origins of FRET-observed nascent chain compaction on the ribosome. *J. Phys. Chem. B* 122(43):9927–37
146. Nissley DA, Vu QV, Trovato F, Ahmed N, Jiang Y, et al. 2020. Electrostatic interactions govern extreme nascent protein ejection times from ribosomes and can delay ribosome recycling. *J. Am. Chem. Soc.* 142(13):6103–10
147. Noel JK, Levi M, Raghunathan M, Lammert H, Hayes RL, et al. 2016. SMOG 2: a versatile software package for generating structure-based models. *PLOS Comput. Biol.* 12(3):e1004794
148. O'Brien EP, Christodoulou J, Vendruscolo M, Dobson CM. 2012. Trigger factor slows co-translational folding through kinetic trapping while sterically protecting the nascent chain from aberrant cytosolic interactions. *J. Am. Chem. Soc.* 134(26):10920–32
149. O'Brien EP, Hsu STD, Christodoulou J, Vendruscolo M, Dobson CM. 2010. Transient tertiary structure formation within the ribosome exit port. *J. Am. Chem. Soc.* 132(47):16928–37
150. Omar SI, Zhao M, Sekar RV, Moghadam SA, Tuszynski JA, Woodside MT. 2021. Modeling the structure of the frameshift-stimulatory pseudoknot in SARS-CoV-2 reveals multiple possible conformers. *PLOS Comput. Biol.* 17(1):e1008603
151. Pape T, Wintermeyer W, Rodnina MV. 1998. Complete kinetic mechanism of elongation factor Tu-dependent binding of aminoacyl-tRNA to the A site of the *E. coli* ribosome. *EMBO J.* 17(24):7490–97
152. Park SJ, Kim YG, Park HJ. 2011. Identification of RNA pseudoknot-binding ligand that inhibits the −1 ribosomal frameshifting of SARS-coronavirus by structure-based virtual screening. *J. Am. Chem. Soc.* 133(26):10094–100
153. Petrone PM, Snow CD, Lucent D, Pande VS. 2008. Side-chain recognition and gating in the ribosome exit tunnel. *PNAS* 105(43):16549–54
154. Polikanov YS, Steitz TA, Innis CA. 2014. A proton wire to couple aminoacyl-tRNA accommodation and peptide-bond formation on the ribosome. *Nat. Struct. Mol. Biol.* 21(9):787–93
155. Qi Y, Ingólfsson HI, Cheng X, Lee J, Marrink SJ, Im W. 2015. CHARMM-GUI Martini Maker for coarse-grained simulations with the Martini force field. *J. Chem. Theory Comput.* 11(9):4486–94
156. Ribeiro JV, Bernardi RC, Rudack T, Stone JE, Phillips JC, et al. 2016. QwikMD—integrative molecular dynamics toolkit for novices and experts. *Sci. Rep.* 6:26536
157. Rico F, Russek A, González L, Grubmüller H, Scheuring S. 2019. Heterogeneous and rate-dependent streptavidin–biotin unbinding revealed by high-speed force spectroscopy and atomistic simulations. *PNAS* 116(14):6594–601
158. Riegger RJ, Caliskan N. 2022. Thinking outside the frame: impacting genomes capacity by programmed ribosomal frameshifting. *Front. Mol. Biosci.* 9:129
159. Robustelli P, Kohlhoff K, Cavalli A, Vendruscolo M. 2010. Using NMR chemical shifts as structural restraints in molecular dynamics simulations of proteins. *Structure* 18(8):923–33
160. Rodnina MV. 2018. Translation in prokaryotes. *Cold Spring Harb. Perspect. Biol.* 10(9):a032664
161. Rodnina MV. 2023. Decoding and recoding of mRNA sequences by the ribosome. *Annu. Rev. Biophys.* 52. In press
162. Rodnina MV, Fischer N, Maracci C, Stark H. 2017. Ribosome dynamics during decoding. *Philos. Trans. R. Soc. B* 372(1716):20160182
163. Rodnina MV, Fricke R, Kuhn L, Wintermeyer W. 1995. Codon-dependent conformational change of elongation factor Tu preceding GTP hydrolysis on the ribosome. *EMBO J.* 14(11):2613–19

164. Rundlet EJ, Holm M, Schacherl M, Natchiar SK, Altman RB, et al. 2021. Structural basis of early translocation events on the ribosome. *Nature* 595(7869):741–45
165. Saio T, Guan X, Rossi P, Economou A, Kalodimos CG. 2014. Structural basis for protein antiaggregation activity of the trigger factor chaperone. *Science* 344(6184):1250494
166. Saio T, Kawagoe S, Ishimori K, Kalodimos CG. 2018. Oligomerization of a molecular chaperone modulates its activity. *eLife* 7:e35731
167. Sanbonmatsu KY. 2012. Computational studies of molecular machines: the ribosome. *Curr. Opin. Struct. Biol.* 22(2):168–74
168. Sanbonmatsu KY. 2019. Large-scale simulations of nucleoprotein complexes: ribosomes, nucleosomes, chromatin, chromosomes and CRISPR. *Curr. Opin. Struct. Biol.* 55:104–13
169. Sanbonmatsu KY, Joseph S, Tung CS. 2005. Simulating movement of tRNA into the ribosome during decoding. *PNAS* 102(44):15854–59
170. Satpati P, Åqvist J. 2014. Why base tautomerization does not cause errors in mRNA decoding on the ribosome. *Nucleic Acids Res.* 42(20):12876–84
171. Schlick T, Zhu Q, Dey A, Jain S, Yan S, Laederach A. 2021. To knot or not to knot: multiple conformations of the SARS-CoV-2 frameshifting RNA element. *J. Am. Chem. Soc.* 143(30):11404–22
172. Schlick T, Zhu Q, Jain S, Yan S. 2021. Structure-altering mutations of the SARS-CoV-2 frameshifting RNA element. *Biophys. J.* 120(6):1040–53
173. Schmeing TM, Huang KS, Kitchen DE, Strobel SA, Steitz TA. 2005. Structural insights into the roles of water and the 2′ hydroxyl of the P site tRNA in the peptidyl transferase reaction. *Mol. Cell* 20(3):437–48
174. Schmeing TM, Voorhees RM, Kelley AC, Gao YG, Murphy FV, et al. 2009. The crystal structure of the ribosome bound to EF-Tu and aminoacyl-tRNA. *Science* 326(5953):688–94
175. Schröder GF, Grubmüller H. 2003. Maximum likelihood trajectories from single molecule fluorescence resonance energy transfer experiments. *J. Chem. Phys.* 119(18):9920–24
176. Schütz S, Sprangers R. 2020. Methyl TROSY spectroscopy: a versatile NMR approach to study challenging biological systems. *Prog. Nuclear Magn. Reson. Spectrosc.* 116:56–84
177. Senn HM, Thiel W. 2009. QM/MM methods for biomolecular systems. *Angew. Chem. Int. Ed.* 48(7):1198–229
178. Sharma PK, Xiang Y, Kato M, Warshel A. 2005. What are the roles of substrate-assisted catalysis and proximity effects in peptide bond formation by the ribosome? *Biochemistry* 44(34):11307–14
179. Shaw DE, Adams PJ, Azaria A, Bank JA, Batson B, et al. 2021. Anton 3: twenty microseconds of molecular dynamics simulation before lunch. In *SC'21: Proceedings of the International Conference for High Performance Computing, Networking, Storage and Analysis*, pp. 1–11. New York: ACM
180. Singh AK, McGoldrick LL, Demirkhanyan L, Leslie M, Zakharian E, Sobolevsky AI. 2019. Structural basis of temperature sensation by the TRP channel TRPV3. *Nat. Struct. Mol. Biol.* 26(11):994–98
181. Small MC, Lopes P, Andrade RB, MacKerell AD. 2013. Impact of ribosomal modification on the binding of the antibiotic telithromycin using a combined grand canonical Monte Carlo/molecular dynamics simulation approach. *PLOS Comput. Biol.* 9(6):e1003113
182. Sothiselvam S, Liu B, Han W, Ramu H, Klepacki D, et al. 2014. Macrolide antibiotics allosterically predispose the ribosome for translation arrest. *PNAS* 111(27):9804–9
183. Stark H, Rodnina MV, Rinke-Appel J, Brimacombe R, Wintermeyer W, Van Heel M. 1997. Visualization of elongation factor Tu on the *Escherichia coli* ribosome. *Nature* 389(6649):403–6
184. Stryer L, Haugland RP. 1967. Energy transfer: a spectroscopic ruler. *PNAS* 58(2):719–26
185. Su T, Cheng J, Sohmen D, Hedman R, Berninghausen O, et al. 2017. The force-sensing peptide VemP employs extreme compaction and secondary structure formation to induce ribosomal stalling. *eLife* 6:e25642
186. Sudhakar S, Kazem M, Tobias A, Jachowski J, Bugiel M, et al. 2021. Germanium nanospheres for ultraresolution picotensiometry of kinesin motors. *Science* 371(6530):eabd9944
187. Tavakoli M, Jazani S, Sgouralis I, Heo W, Ishii K, et al. 2020. Direct photon-by-photon analysis of time-resolved pulsed excitation data using Bayesian nonparametrics. *Cell Rep. Phys. Sci.* 1(11):100234
188. Thiel W. 2014. Semiempirical quantum–chemical methods. *Wiley Interdiscip. Rev. Comput. Mol. Sci.* 4(2):145–57

189. Tian P, Steward A, Kudva R, Su T, Shilling PJ, et al. 2018. Folding pathway of an Ig domain is conserved on and off the ribosome. *PNAS* 115(48):E11284–93
190. Trabuco LG, Schreiner E, Eargle J, Cornish P, Ha T, et al. 2010. The role of L1 stalk–tRNA interaction in the ribosome elongation cycle. *J. Mol. Biol.* 402(4):741–60
191. Trabuco LG, Villa E, Mitra K, Frank J, Schulten K. 2008. Flexible fitting of atomic structures into electron microscopy maps using molecular dynamics. *Structure* 16(5):673–83
192. Trovato F, O'Brien EP. 2016. Insights into cotranslational nascent protein behavior from computer simulations. *Annu. Rev. Biophys.* 45:345–69
193. Tuckerman M. 2010. *Statistical Mechanics: Theory and Molecular Simulation*. Oxford, UK: Oxford Univ. Press
194. Uusitalo JJ, Ingólfsson HI, Marrink SJ, Faustino I. 2017. Martini coarse-grained force field: extension to RNA. *Biophys. J.* 113(2):246–56
195. Vaiana AC, Sanbonmatsu KY. 2009. Stochastic gating and drug–ribosome interactions. *J. Mol. Biol.* 386(3):648–61
196. van Gunsteren WF, Berendsen HJ. 1990. Computer simulation of molecular dynamics: methodology, applications, and perspectives in chemistry. *Angew. Chem. Int. Ed.* 29(9):992–1023
197. Volkhardt A, Grubmüller H. 2022. Estimating ruggedness of free-energy landscapes of small globular proteins from principal component analysis of molecular dynamics trajectories. *Phys. Rev. E* 105(4):044404
198. Voorhees RM, Weixlbaumer A, Loakes D, Kelley AC, Ramakrishnan V. 2009. Insights into substrate stabilization from snapshots of the peptidyl transferase center of the intact 70S ribosome. *Nat. Struct. Mol. Biol.* 16(5):528–33
199. Vu QV, Jiang Y, Li MS, O'Brien EP. 2021. The driving force for co-translational protein folding is weaker in the ribosome vestibule due to greater water ordering. *Chem. Sci.* 12(35):11851–57
200. Wallin G, Åqvist J. 2010. The transition state for peptide bond formation reveals the ribosome as a water trap. *PNAS* 107(5):1888–93
201. Wallin G, Kamerlin SCL, Åqvist J. 2013. Energetics of activation of GTP hydrolysis on the ribosome. *Nat. Commun.* 4:1733
202. Wang A, Levi M, Mohanty U, Whitford PC. 2022. Diffuse ions coordinate dynamics in a ribonucleoprotein assembly. *J. Am. Chem. Soc.* 144(21):9510–22
203. Wang X, Kirkpatrick JP, Launay HM, de Simone A, Häussinger D, et al. 2019. Probing the dynamic stalk region of the ribosome using solution NMR. *Sci. Rep.* 9:13528
204. Warias M, Grubmüller H, Bock LV. 2020. tRNA dissociation from EF-tu after GTP hydrolysis: primary steps and antibiotic inhibition. *Biophys. J.* 118(1):151–61
205. Warshel A. 2003. Computer simulations of enzyme catalysis: methods, progress, and insights. *Annu. Rev. Biophys. Biomol. Struct.* 32:425–43
206. Waudby CA, Dobson CM, Christodoulou J. 2019. Nature and regulation of protein folding on the ribosome. *Trends Biochem. Sci.* 44(11):914–26
207. Waudby CA, Włodarski T, Karyadi ME, Cassaignau AM, Chan SH, et al. 2018. Systematic mapping of free energy landscapes of a growing filamin domain during biosynthesis. *PNAS* 115(39):9744–49
208. White KH, Orzechowski M, Fourmy D, Visscher K. 2011. Mechanical unfolding of the Beet Western Yellow Virus −1 frameshift signal. *J. Am. Chem. Soc.* 133(25):9775–82
209. Whitford PC, Blanchard SC, Cate JHD, Sanbonmatsu KY. 2013. Connecting the kinetics and energy landscape of tRNA translocation on the ribosome. *PLOS Comput. Biol.* 9(3):e1003003
210. Whitford PC, Geggier P, Altman RB, Blanchard SC, Onuchic JN, Sanbonmatsu KY. 2010. Accommodation of aminoacyl-tRNA into the ribosome involves reversible excursions along multiple pathways. *RNA* 16(6):1196–204
211. Wilson DN, Arenz S, Beckmann R. 2016. Translation regulation via nascent polypeptide-mediated ribosome stalling. *Curr. Opin. Struct. Biol.* 37:123–33
212. Wruck F, Katranidis A, Nierhaus KH, Büldt G, Hegner M. 2017. Translation and folding of single proteins in real time. *PNAS* 114(22):E4399–407
213. Wruck F, Tian P, Kudva R, Best RB, von Heijne G, et al. 2021. The ribosome modulates folding inside the ribosomal exit tunnel. *Commun. Biol.* 4:523

214. Xu Y, Vanommeslaeghe K, Aleksandrov A, MacKerell AD Jr., Nilsson L. 2016. Additive CHARMM force field for naturally occurring modified ribonucleotides. *J. Comput. Chem.* 37(10):896–912
215. Yang H, Bandarkar P, Horne R, Leite VB, Chahine J, Whitford PC. 2019. Diffusion of tRNA inside the ribosome is position-dependent. *J. Chem. Phys.* 151(8):085102
216. Yang YI, Shao Q, Zhang J, Yang L, Gao YQ. 2019. Enhanced sampling in molecular dynamics. *J. Chem. Phys.* 151(7):070902
217. Ye W, Götz M, Celiksoy S, Tüting L, Ratzke C, et al. 2018. Conformational dynamics of a single protein monitored for 24 h at video rate. *Nano Lett.* 18(10):6633–37
218. Zhang J, Pan X, Yan K, Sun S, Gao N, Sui SF. 2015. Mechanisms of ribosome stalling by SecM at multiple elongation steps. *eLife* 4:e09684
219. Zhang K, Zheludev IN, Hagey RJ, Haslecker R, Hou YJ, et al. 2021. Cryo-EM and antisense targeting of the 28-kDa frameshift stimulation element from the SARS-CoV-2 RNA genome. *Nat. Struct. Mol. Biol.* 28(9):747–54
220. Zhang Y, Hong S, Ruangprasert A, Skiniotis G, Dunham CM. 2018. Alternative mode of E-site tRNA binding in the presence of a downstream mRNA stem loop at the entrance channel. *Structure* 26(3):437–45.e3
221. Zhong Z, Yang L, Zhang H, Shi J, Vandana JJ, et al. 2016. Mechanical unfolding kinetics of the SRV-1 gag-pro mRNA pseudoknot: possible implications for −1 ribosomal frameshifting stimulation. *Sci. Rep.* 6:39549
222. Zhu X, Lopes PE, MacKerell AD Jr. 2012. Recent developments and applications of the CHARMM force fields. *Wiley Interdiscip. Rev. Comput. Mol. Sci.* 2(1):167–85
223. Zimmer MH, Niesen MJ, Miller TF III. 2021. Force transduction creates long-ranged coupling in ribosomes stalled by arrest peptides. *Biophys. J.* 120(12):2425–35